NASA CR-134684

MIXED MODE STRESS INTENSITY FACTORS FOR SEMIELLIPTICAL SURFACE CRACKS

by

F. W. Smith and D. R. Sorensen

COLORADO STATE UNIVERSITY

prepared for

NATIONAL AERONAUTICS AND SPACE ADMINISTRATION

NASA Lewis Research Center

Grant NGL 06-002-063

John A. Misencik, Project Manager

NOTICE

This report was prepared as an account of Government-sponsored work. Neither the United States, nor the National Aeronautics and Space Administration (NASA), nor any person acting on behalf of NASA:

A.) Makes any warranty or representation, expressed or implied, with respect to the accuracy, completeness, or usefulness of the information contained in this report, or that the use of any information, apparatus, method, or process disclosed in this report may not infringe privately-owned right; or

B.) Assumes any liabilities with respect to the use of, or for damages resulting from the use of, any information, apparatus, method or process disclosed in this report.

As used above, "person acting on behalf of NASA" includes any employee or contractor of NASA, or employee of such contractor, to the extent that such employee or contractor of NASA or employee of such contractor prepares, disseminates, or provides access to any information pursuant to his employment or contract with NASA, or his employment with such contractor.

Requests for copies of this report should be referred to

National Aeronautics and Space Administration
Scientific and Technical Information Facility
P. O. Box 33
College Park, Md. 20740

1. Report No.	2. Government Accession No	3. Recipient's Catalog No
NASA CR-134684		

4. Title and Subtitle	5. Report Date
Mixed Mode Stress Intensity Factors for Semielliptical Surface Cracks	June 1974
	6. Performing Organization Code

7. Author(s)	8. Performing Organization Report No.
F. W. Smith and D. R. Sorensen	
	10. Work Unit No.

9. Performing Organization Name and Address	11. Contract or Grant No.
Department of Mechanical Engineering Colorado State University Fort Collins, Colorado 80523	NGL 06-002-063
	13. Type of Report and Period Covered
12. Sponsoring Agency Name and Address	Contractor Report
National Aeronautics and Space Administration Lewis Research Center 21000 Brookpark Road Cleveland, Ohio, 44135	14. Sponsoring Agency Code

15. Supplementary Notes

Project Manager, John A. Misencik,
Materials and Structures Division
NASA Lewis Research Center

16. Abstract

The three-dimensional equations of elasticity are solved for a flat elliptical crack which has nonuniform shear stresses applied to its surfaces. An alternating method is used to determine the mode two and mode three stress intensity factors for a semielliptical surface crack in the surface of a finite thickness solid. These stress intensity factors are presented as a function of position along the crack border for a number of crack shapes and crack depths.

This same technique is followed to determine the mode one stress intensity factors for the semielliptical surface crack which has normal loading applied to its surfaces. Mode one stress intensity factors are presented and compared with the results obtained from previous work.

17. Key Words (Suggested by Author(s))	18. Distribution Statement
Fracture Mechanics Mixed Mode Fracture Stress Intensity Factors Surface Cracks	Unclassified, Unlimited

19. Security Classif. (of this report)	20. Security Classif. (of this page)	21. No. of Pages	22. Price*
Unclassified	Unclassified	97	$3.00

* For sale by the National Technical Information Service, Springfield, Virginia 22151

TABLE OF CONTENTS

LIST OF FIGURES

INTRODUCTION

1.0 Background

For years much of the fracture mechanics research, both theoretical and experimental, has been devoted to the study of problems in which the loads were applied in a direction perpendicular to the plane of the crack. Studies of this type provide valid information for solely mode one, or opening mode problems.

A knowledge of only mode one displacements is inadequate or insufficient to perform the proper design analyses required for the structures being considered today. Factors such as complex loadings, nonuniform loadings, and the nonalignment of loadings and crack geometries demand that a study of mixed mode fracture mechanics be accomplished to insure that the maximum possible structural integrity is attained. Mixed mode problems arise frequently in bridges, pipes, pressure vessels, and aircraft and aerospace structures. The necessity for using high strength alloys in the fabrication of many structures of this type intensifies the requirement for adequate mixed mode fracture mechanics analysis since many of these alloys are often quite brittle and sensitive to the presence of flaws or mechanical defects.

An example of a situation in which fracture mechanics considerations will be exercised is in the design of the space shuttle structure. Many components of the space shuttle will be reused a number of times and be exposed to hostile environmental effects, so a proper design analysis must be made which will include adequate assurance that the desired life is not threatened by possible crack growth. Mixed mode fracture mechanics considerations would be of less consequence if the

structural components were to be used only once, but they gain increased magnitudes of importance when the components must withstand a number of launches and recoveries. It is for considerations such as these that a study of mixed mode fracture mechanics problems was undertaken.

Part I of this report is devoted to the study of a semielliptical surface flaw which has nonuniform shear loading applied to the surfaces in either of two directions, parallel or perpendicular to the major axis of the ellipse. An alternating method is used to calculate the mode two and mode three stress intensity factors. These stress intensity factors are presented as a function of position along the crack border for a number of crack shapes and crack depths. No similar results have heretofore been obtained for this problem.

A number of studies have been made for an elliptical crack in an infinite solid and a semielliptical surface flaw in a finite solid, both of which are subjected to uniaxial tension. However, no valid solution exists for a semielliptical surface flaw having small depth to length ratios, a/2c, which penetrates the solid with large depth to thickness ratios, a/t. Kobayashi (1)* has stated that semielliptical surface flaws with a/2c = 0.12 to 0.2 with depth ratios a/t = 0.9 are probably the most critical problems in applied fracture mechanics without an adequate solution. Part II of this report is devoted to the study of semielliptical surface flaws subjected to normal loading. Results of this study were presented in Technical Report No. 4 but are included

*Numbers in parentheses refer to references at the end of the report.

here to allow the presentation of additional computations made since the publication of that report.

2.0 Previous Work

Inglis (2) in 1913 presented the initial analytical work leading to the present day concepts of fracture mechanics. He studied the stresses in the vicinity of an elliptical hole which, in the limit, becomes a sharp crack. This work then provided Griffith (3) with the background necessary to postulate his theory of crack propagation based on a balance between released elastic strain energy and absorbed surface energy.

Much of the initial fracture mechanics work was done on two-dimensional problems, but in 1945 Sneddon (4) formulated the axi-symmetric three-dimensional problem of a circular flat crack in an infinite solid with uniform normal pressure applied to its surfaces. In 1960 Green and Sneddon (5) solved a similar problem for an elliptical crack embedded in an infinite solid, and in 1971 Shah and Kobayashi (6) extended this solution to the case of an embedded elliptical crack under arbitrary normal loading. All of these solutions dealt only with embedded cracks.

The solution of Green and Sneddon (5) was used by Irwin (7) in 1966 to estimate stress intensity factors for a semielliptical crack in the surface of a flat plate. Smith (8, 9) in 1966 presented the solution to the problem involving a semicircular surface crack located at a free surface of a half-space and loaded with an arbitrary normal pressure. He used an alternating technique originally used by Lachenbruch (10) to remove and calculate the effects of normal stresses on the free surface.

Smith and Alavi (11, 12, 13) later solved the problem of a circular crack embedded in a semi-infinite solid, and the problem of a part-circular crack in the surface of a semi-infinite solid. Thresher and Smith (14, 15) in 1972 extended this work to solve the problem of a part-circular surface flaw in a finite thickness solid. In 1973, Shah and Kobayashi gave solutions to the problems of an embedded elliptical crack approaching the free surface of a semi-infinite solid subjected to uniform tension (16, 17) and linearly varying pressure (18). All of the solutions mentioned above were for normal loading of the crack surface, and thus involved only mode one displacements and stress intensity factors.

Much less work has been done for the three-dimensional problems involving cracks which have shear loading applied to their surfaces, although some work has been done for cracks embedded in infinite bodies. Segedin (19) in 1950 presented a solution for an embedded circular crack subjected to a uniform shear stress. This same problem was also solved by Westmann (20), while Shelby (21) discussed it as a special case of his more general solution for an ellipsoidal inclusion in an infinite elastic medium.

Kassir and Sih (22) in 1966 formulated the problem of an embedded elliptical crack in an infinite solid, subjected to uniform shear applied in any direction. They studied the stress field near the crack border, and presented mode two and mode three stress intensity factors as functions of position along the crack border.

3.0 Objectives of the Report

The objectives of this report are two-fold. The first objective is to present the stress intensity factors for a semielliptical surface crack in a finite thickness solid subjected to shear loading.

The second objective is to present stress intensity factors for a semielliptical surface crack which has normal loading applied to its surfaces. This work is the first presentation of an analysis of this problem which includes all known elastic effects, and it covers ranges of crack depth and shape for which results of direct analysis are not available.

PART I--SHEAR LOADING OF A SEMIELLIPTICAL SURFACE CRACK

Chapter 1

THE SHEAR LOADING PROBLEM

1.0 General Statement of the Surface Crack Problem

Consider a semielliptical surface crack located in the front surface of a finite thickness slab, as shown in Fig. 1. The crack is considered to lie on the plane defined by $z = 0$, and has a semiminor axis "b" located along the y-axis, and a semimajor axis "a" located along the x-axis.

The problem is to determine the stress intensity factor along the periphery of the crack when the surface of the crack is subjected to nonuniform shear stresses τ_{zx} and τ_{zy}, the positive directions of which are shown in Fig. 1. Boundary conditions for this problem are determined from a consideration of the conditions of skew symmetry of the displacements of the problem. These boundary conditions are:

$$\sigma_{zz} = 0, \quad (z = 0) \tag{1.1}$$

and

$$u = v = 0, \quad \left(\frac{x^2}{a^2} + \frac{y^2}{b^2} > 1; \quad z = 0 \right) \tag{1.2}$$

where u and v are the displacements in the x and y directions, respectively. The front and back surfaces of the body are considered to be free of stresses.

In addition, the shear stresses on the surface of the crack can be expressed by the following series representations:

$$\tau_{zx} = \sum_{m=0}^{3} \sum_{n=0}^{3} A_{mn} x^m y^n ,$$

$$\left(\frac{x^2}{a^2} + \frac{y^2}{b^2} \leq 1; \quad z = 0 \right) \qquad (1.3)$$

$$\tau_{zy} = \sum_{m=0}^{3} \sum_{n=0}^{3} B_{mn} x^m y^n ,$$

where $m + n \leq 3$. The sum, $m + n$, is limited to being less than or equal to three because of the enormous quantity of work necessary to derive the equations for the stresses and stress intensity factors.

2.0 The Method of Solution

The method of solution which will be used is an alternating technique similar to the one which has been used by Thresher and Smith (15), and in a slightly different manner by Shah and Kobayashi (17). Two elastic solutions are required to apply this technique. The results from each solution are superposed to yield a solution to the problem. These two solutions will be referred to as Solution 1 and Solution 2 as follows:

Solution 1. The determination of the stresses at any point in an infinite solid due to the presence of an elliptical crack in the infinite solid. The crack surface is subjected to variable shear stresses.

Solution 2. The determination of the stresses within a semi-infinite body subjected to uniform normal and shear stress applied over a rectangular portion of the surface.

2.1 Elastic Solution of a Crack in an Infinite Solid

Solution 1 represents the elastic solution of an elliptical crack in an infinite solid subjected to nonuniform shear stresses. These shear stresses can be applied to the surface of the crack parallel to the minor axis or the major axis, or parallel to both axes simultaneously. This method solves the three-dimensional equations of elasticity for the displacements and the stresses at any particular point within the infinite body. Additional derivations are made for the equations which define the stress intensity factors as functions of position along the crack border. The derivations and the explanation of this method are accomplished in Chapter 2.

2.2 The Half-Space Solution

Solution 2 utilizes the general formulation of a half-space problem by Love (23, 24). This is a solution for stresses in a half-space due to normal and shear tractions applied to a rectangular portion of the surface.

For the problem under consideration here, the shear stresses τ_{zx} and τ_{zy} had to be calculated from the Love formulation on the face of the crack. This had not been done before so it was necessary to derive the equations using Love's general formulation as a beginning point. The skew symmetry conditions of this problem preclude the presence of any residual normal stresses σ_{zz} on the face of the crack, so it was not necessary to calculate this component.

The details of the solution are presented in Chapter 3.

2.3 The Alternating Method

The alternating method which is applied to the semielliptical surface crack problem works in the following way:

1. The shear loading, τ_{zx} or τ_{zy}, is applied to the crack surface as prescribed from the statement of the particular problem being solved. Solution 1 is used to compute the normal and shearing stresses at points on a plane in the infinite solid at the location of the front surface.
2. The front surface of the body must be free of stresses, so the stresses produced in the previous step must be removed. This requires that opposing surface tractions be applied on the plane of an uncracked half-space. This is done by dividing the front surface into a number of rectangular areas and applying stresses to each area which are equal in magnitude but opposite in sign to the stresses computed at the center of each rectangle in Step 1. Solution 2 is then used to compute the shear stresses τ_{zx} and τ_{zy} at 96 points at the location of the crack surface in the half space. The effects of all surface rectangles are included by summing over the entire number of rectangles used on the surface. The result of this is a secondary residual stress which is now generated on the crack surface.

   Figure 2 shows a typical arrangement of surface rectangles used in the analysis. This pattern is the one which appears in the first quadrant and is repeated in each of the other three quadrants.
3. The stress residuals which have now been produced on the crack surface must be removed in order that the boundary conditions on the crack surface can be met. This is done by applying opposing stresses on the crack surface. The polynomial

equations (1.3) for τ_{zx} and τ_{zy} are least square fitted to the values of the stress residuals at the 96 points on the crack surface shown in Fig. 3.

The change in the stress intensity factors ΔK_2 and ΔK_3 caused by the application of these opposing stresses is calculated and added to the stress intensity factors caused by the initial loading. Solution 1 is again used to compute the stresses on the front surface if more than one iteration is desired on that surface. Either one or two iterations of this kind are done with the front surface, storing the stress residuals applied to the crack surface as well as the stress residuals applied to the front surface.

4. When stress residuals are applied to the front surface, stresses are produced at the location of the back surface. These stresses must also be accounted for during the application of the alternating technique. The applied stresses on the front surface are used to calculate the stresses on the back surface, using Solution 2, and stresses of the opposite sign are then applied to the back surface. This, in turn, causes some additional stress residuals on the crack which must be removed, and the change in the stress intensity factors ΔK_2 and ΔK_3 is once again calculated. This change is then added to the running sum of each stress intensity factor which was calculated from the initial loading plus the contributions of any subsequent iterations.
5. The same steps which have been accomplished between and crack and the front surface are now done between the crack and the

back surface, and a process similar to the one between the front and the back surface is now performed between the back and front surface.

Steps one through five constitute one cycle of iteration. Several cycles are executed until the changes in K_2 and K_3 from each step are negligible as compared to the values caused by the initial loading. The final stress intensity factors are the sum of all the stress intensities due to the initially prescribed crack surface stresses plus the contributions due to all the stress residuals which are applied at the crack surface.

This procedure is extremely complicated and time-consuming when it is considered that a large number of rectangles are used on each surface, and 96 points are used on the crack face. For this reason, all such calculations were programmed and performed on the digital computer.

Chapter 2

THE ELLIPTICAL CRACK WITH NONUNIFORM SHEAR LOADING

1.0 The Problem and its Boundary Conditions

The problem, referred to earlier as "Solution 1", is illustrated in Fig. 4, and is a flat elliptical crack embedded in an infinite solid. The crack has a semiminor axis "b" located along the y-axis, and a semimajor axis "a" located along the x-axis. The plane of the crack is considered to lie on the plane defined by $z = 0$. The surface of the crack is subjected to nonuniform shear stresses τ_{zx} and τ_{zy}, the positive directions of which are shown in Fig. 4.

Considerations of the conditions of skew symmetry of the displacements lead to the following boundary conditions:

$$\sigma_{zz} = 0 , \qquad (z = 0) \tag{2.1}$$

and

$$u = v = 0 , \quad \left(\frac{x^2}{a^2} + \frac{y^2}{b^2} > 1; \quad z = 0 \right) \tag{2.2}$$

where u and v are the displacements in the x and y-directions, respectively. It is assumed that the shear stresses applied to the surface of the crack are expressible in terms of a polynomial of x and y as

$$\tau_{zx} = \sum_{m=0}^{3} \sum_{n=0}^{3} A_{mn} x^m y^n ,$$

$$\left(\frac{x^2}{a^2} + \frac{y^2}{b^2} \leq 1; \quad z = 0 \right) \tag{2.3}$$

$$\tau_{zy} = \sum_{m=0}^{3} \sum_{n=0}^{3} B_{mn} x^m y^n ,$$

where $m + n \leq 3$.

All stresses are assumed to vanish at large distances from the crack.

2.0 Stress Functions, Displacements and Stresses

Kassir and Sih (22) formulated the problem of an elliptical crack subjected to uniform shear applied in any direction as a mixed boundary value problem. They were able to satisfy the three-dimensional equations of elasticity through the appropriate selection of two harmonic stress functions, f and g. These functions satisfy Laplace's equations

$$\nabla^2 f = \nabla^2 g = 0. \tag{2.4}$$

Navier's displacement equations of equilibrium are satisfied by the harmonic functions, f and g. Define

$$F = \frac{\partial f}{\partial x} + \frac{\partial g}{\partial y} \quad \text{and} \quad \nabla^2 F = 0. \tag{2.5}$$

The rectangular components u, v, and w of the displacement vector are given in terms of the harmonic functions as:

$$u = -2(1 - \eta) \frac{\partial f}{\partial z} + z \frac{\partial F}{\partial x} \tag{2.6a}$$

$$v = -2(1 - \eta) \frac{\partial g}{\partial z} + z \frac{\partial F}{\partial y} \tag{2.6b}$$

$$w = -(1 - 2\eta) F + z \frac{\partial F}{\partial z} \tag{2.6c}$$

where u, v, and w are the displacement components in the x, y, and z directions, respectively, and η is Poisson's ratio. The strain-displacement equations may be applied to the displacements to yield the strains, and in turn the stress-strain relationships for linear elasticity may be used to obtain the stresses in terms of the stress functions f and g to be

$$\frac{\sigma_{xx}}{2G} = -2(1 - \eta) \frac{\partial^2 f}{\partial x \partial z} - 2\eta \frac{\partial F}{\partial z} + z \frac{\partial^2 F}{\partial x^2} \tag{2.7a}$$

$$\frac{\sigma_{yy}}{2G} = -2(1 - \eta) \frac{\partial^2 g}{\partial y \partial z} - 2\eta \frac{\partial F}{\partial z} + z \frac{\partial^2 F}{\partial y^2} \tag{2.7b}$$

$$\frac{\sigma_{zz}}{2G} = z \frac{\partial^2 F}{\partial z^2} \tag{2.7c}$$

$$\frac{\tau_{xy}}{2G} = -(1 - \eta) \frac{\partial}{\partial z} \left(\frac{\partial f}{\partial y} + \frac{\partial g}{\partial x} \right) + z \frac{\partial^2 F}{\partial x \partial y} \tag{2.7d}$$

$$\frac{\tau_{xz}}{2G} = -(1 - \eta) \frac{\partial^2 f}{\partial z^2} + \eta \frac{\partial F}{\partial x} + z \frac{\partial^2 F}{\partial x \partial z} \tag{2.7e}$$

$$\frac{\tau_{yz}}{2G} = -(1 - \eta) \frac{\partial^2 g}{\partial z^2} + \eta \frac{\partial F}{\partial y} + z \frac{\partial^2 F}{\partial y \partial z} \tag{2.7f}$$

where G is the shear modulus.

It has been found convenient in solving boundary value problems of this nature to introduce the ellipsoidal coordinate system λ, μ, and ν where these ellipsoidal coordinates are roots of the equation

$$1 - \frac{x^2}{a^2+s} - \frac{y^2}{b^2+s} - \frac{z^2}{s} = 0. \tag{2.8}$$

The ellipsoidal coordinates λ, μ and ν are related to the cartesian coordinates x, y and z by the transformation equations:

$$a^2(a^2-b^2)\, x^2 = (a^2+\lambda)\,(a^2+\mu)\,(a^2+\nu) \tag{2.9a}$$

$$b^2(b^2-a^2)\, y^2 = (b^2+\lambda)\,(b^2+\mu)\,(b^2+\nu) \tag{2.9b}$$

$$a^2 b^2 z^2 = \lambda\mu\nu \tag{2.9c}$$

where the values of the coordinates are limited to the standard restrictions:

$$-a^2 \leq \nu \leq -b^2 \leq \mu \leq 0 \leq \lambda < \infty \tag{2.10}$$

In these coordinates, on the plane z = 0, the interior of the crack is described by $\lambda = 0$ while the region exterior to the crack is described by $\mu = 0$.

Segedin (25) suggested the use of a series of functions which satisfy (2.4) and have properties which make it possible to satisfy boundary conditions of the type required by (2.1), (2.2), and (2.3). Shah and Kobayashi (6) used them to develop the solution for an embedded elliptical crack subjected to nonuniform normal loading. These functions are used here in a similar way to solve this problem and are expressed in the form

$$\begin{pmatrix} f \\ g \end{pmatrix} = \sum_{m=0}^{3} \sum_{n=0}^{3} \begin{pmatrix} a_{mn} \\ b_{mn} \end{pmatrix} \frac{\partial^{m+n} V^{(m+n+1)}}{\partial x^m \partial y^n} \tag{2.11}$$

where $m + n \leq 3$,

$$V^{(j)} = \int_{\lambda}^{\infty} \frac{\omega^j(s)}{\sqrt{Q(s)}} ds \tag{2.12}$$

$$\omega(s) = 1 - \frac{x^2}{a^2+s} - \frac{y^2}{b^2+s} - \frac{z^2}{s} \tag{2.13}$$

and

$$Q(s) = s(a^2+s)\ (b^2+s). \tag{2.14}$$

Segedin (25) showed that $V^{(n)}$ is a harmonic potential function. Since $V^{(n)}$ is harmonic, the stress functions, f and g, are also harmonic and therefore satisfy the governing differential equations (2.4).

3.0 Satisfying the Boundary Conditions

The boundary conditions, as defined in (2.1), (2.2), and (2.3), must now be satisfied to complete the formal elastic solution. Equation (2.1) states the first boundary condition as being $\sigma_{zz} = 0$ on

the plane z = 0. It is obvious from (2.7c) that this boundary condition is identically satisfied at any point on the plane z = 0.

Equation (2.2) states that the displacements in the x and y-direction, u and v, are equal to zero outside the ellipse on the plane z = 0. The substitution of this equation into (2.6a) and (2.6b) yields:

$$\frac{\partial f}{\partial z} = \frac{\partial g}{\partial z} = 0 \tag{2.15}$$

Segedin (25) showed that the z-derivative of the function $V^{(m)}$ vanishes on the plane z = 0 in the region outside of the ellipse. From (2.11) it can be seen that if $\partial V^{(m)}/\partial z$ vanishes outside the ellipse for z = 0, then $\partial f/\partial z$ and $\partial g/\partial z$ must likewise vanish, thus satisfying the boundary conditions (2.2).

The final task remaining in satisfying the boundary conditions is that of satisfying (2.3) for τ_{zx} and τ_{zy} inside the crack on the plane z = 0. This was done by deriving the expressions for the stress components τ_{zx} and τ_{zy} on the plane z = 0 inside of the ellipse, using (2.7e) and (2.7f), for each term in the polynomial which is produced by (2.11). The result was a polynomial expression corresponding to each one of the ten independent a_{mn} coefficients and the ten independent b_{mn} coefficients. To satisfy the shear stress boundary conditions, coefficients of similar powers of $x^m y^n$ were collected from all the calculations described above and equated to the corresponding coefficient from (2.3). This resulted in the following matrix equation:

$$[K_{ij}]\begin{Bmatrix} a_{00} \\ a_{10} \\ a_{01} \\ a_{20} \\ a_{11} \\ a_{02} \\ a_{12} \\ a_{21} \\ a_{30} \\ a_{03} \\ b_{mn} \end{Bmatrix} = \begin{Bmatrix} A_{00} \\ A_{10} \\ A_{01} \\ A_{20} \\ A_{11} \\ A_{02} \\ A_{12} \\ A_{21} \\ A_{30} \\ A_{03} \\ B_{mn} \end{Bmatrix} \tag{2.16}$$

In the column matrices, the terms b_{mn} and B_{mn} are permuted in an identical manner to the a_{mn} and A_{mn} terms, which are shown as the top half of the column matrices. The square matrix K_{ij} is a 20 x 20 matrix and nonzero terms of this matrix are tabulated in Appendix I.

The solution to a typical problem would require that the A_{mn} and B_{mn} coefficients in the right-hand column matrix be known or specified for the particular problem being solved. It is quite likely that the problem being solved would require only a portion of these coefficients to be nonzero. It is also quite likely that the symmetry or skew-symmetry of the stresses being used could preclude the necessity for using all twenty of the coefficients. Equation (2.16) may be solved for the a_{mn} and b_{mn} coefficients. These would be substituted into (2.11) and then into (2.5) and (2.7) to calculate the stresses, and into (2.6) to compute the displacements.

This completes the formal solution to the three-dimensional equations of elasticity.

4.0 Stress Intensity Factors

The mode two and mode three stress intensity factors would be of more importance to the designer than would the stresses or the displacements near the crack. These stress intensity factors, when defined as a function of position along the crack border, would be used with a suitable failure criterion to help accomplish the design of mechanical parts loaded with nonuniform shear stresses.

4.1 Definition of K_2 and K_3

Mode two and mode three stress intensity factors have been computed for each a_{mn} and b_{mn} term in the stress functions of (2.11). This was done by computing the following limits for mode two and mode three stress intensities, respectively:

$$K_2 = \lim_{r \to 0} \left[(2\pi r)^{\frac{1}{2}} \tau_{zn} \Big|_{z=0} \right]$$
$$K_3 = \lim_{r \to 0} \left[(2\pi r)^{\frac{1}{2}} \tau_{zt} \Big|_{z=0} \right] \qquad (2.17)$$

Figure 5 illustrates the terms used to define K_2 and K_3 in (2.17). The direction normal to the crack front is defined as n, while the direction tangential to the crack front is defined as t. The angle ϕ is the parametric angle of the ellipse, and the angle β is the angle between the x-axis and the outward normal vector. It should be noted that the angle ϕ locates a point along the border of the ellipse which does not in general coincide with the intersection of the radial line with the ellipse. In these expressions, r is the distance from the crack tip

measured along an outward normal, and τ_{zn} and τ_{zt} refer to the stresses in the normal and tangential directions, respectively.

4.2 Derivations of Stress Intensity Factors

Mode two and mode three stress intensity factors, K_2 and K_3, are calculated for every coefficient a_{mn} and b_{mn}. In the following paragraphs a calculation of the stress intensity factors corresponding to the coefficient a_{10} will be done to illustrate the procedure.

The first step is to compute the stress components τ_{zx} and τ_{zy} on the plane $z = 0$ outside the crack. Equation (2.11) is substituted into (2.7e) and (2.7f) to calculate these stresses. The use of Leibnitz' rule for differentiating integrals leads to:

$$\frac{1}{2G}\,\tau_{zx}\Big|_{z=0} = -8(1-\eta)\,a_{10} \times \Gamma_4\Big|_{\substack{z=0\\ \mu=0}} + 8\eta a_{10} \times \Gamma_5\Big|_{\substack{z=0\\ \mu=0}} \tag{2.18}$$

$$\frac{1}{2G}\,\tau_{zy}\Big|_{z=0} = 8\eta a_{10}{}^{y}\,\Gamma_6\Big|_{\substack{z=0\\ \mu=0}} \tag{2.19}$$

where the Γ_i-terms are shorthand notation for:

$$\Gamma_4 = \int_{\lambda}^{\infty} \frac{ds}{s(a^2+s)\sqrt{Q(s)}} - \frac{z}{\lambda(a^2+\lambda)\sqrt{Q(\lambda)}}\,\frac{\partial\lambda}{\partial z} \tag{2.20}$$

$$\Gamma_5 = 3\int_{\lambda}^{\infty} \frac{ds}{(a^2+s)^2\sqrt{Q(s)}} - \frac{x}{(a^2+\lambda)^2\sqrt{Q(\lambda)}}\,\frac{\partial\lambda}{\partial x} \tag{2.21}$$

$$\Gamma_6 = \int_{\lambda}^{\infty} \frac{ds}{(a^2+s)(b^2+s)\sqrt{Q(s)}} - \frac{x}{(a^2+\lambda)(b^2+\lambda)\sqrt{Q(\lambda)}}\,\frac{\partial\lambda}{\partial x} \tag{2.22}$$

Byrd and Friedman's (26) book is used to calculate the above integrals directly in terms of elliptic integrals and Jacobian elliptic

functions. The derivates of λ may be obtained by differentiating (2.9a), (2.9b), and (2.9c). Equations (2.20), (2.21), and (2.22) become

$$\Gamma_4 = \frac{2}{a^5 k^2 k'^2}\left[(1-2k^2)E(u_1) + k^2 dnu_1 tnu_1 - k'^2 u_1\right] - \frac{2z^2(b^2+\lambda)}{\lambda\sqrt{Q(\lambda)}\,(\lambda-\mu)\,(\lambda-\nu)} \tag{2.23}$$

$$\Gamma_5 = \frac{2}{a^5 k^4}\left[(2+k^2)u_1 - 2(1+k^2)E(u_1) + k^2 snu_1 cnu_1 dnu_1\right] - \frac{2x^2\lambda(b^2+\lambda)}{(a^2+\lambda)^2\sqrt{Q(\lambda)}\,(\lambda-\mu)\,(\mu-\nu)} \tag{2.24}$$

$$\Gamma_6 = \frac{2}{a^5 k'^2 k^4}\left[(1+k'^2)E(u_1) - 2k'^2 u_1 - k^2 snu_1 cdu_1\right] - \frac{2x^2\lambda}{(a^2+\lambda)\sqrt{Q(\lambda)}\,(\lambda-\mu)\,(\lambda-\nu)} \tag{2.25}$$

where $E(u_1)$ is the incomplete elliptic integral of the second kind. The modulus k and the complementary modulus k' are defined by

$$k^2 = 1 - b^2/a^2;\ k' = b/a \tag{2.26}$$

The functions sn, cn and dn are Jacobian elliptic functions and u_1 represents the incomplete elliptic integral of the first kind. To find the limiting form of the stresses near the crack tip it is necessary to set $\mu = 0$, and approach the crack tip. As r, the distance from the crack tip, approaches zero the following limiting expressions are applicable:

$$\lambda \to 2abr\,\Phi^{-\frac{1}{2}} ; \qquad \mu = 0 ; \qquad \nu \to -\phi$$

$$snu_1 \to 1 ; \qquad dnu_1 \to b/a ; \qquad cnu_1 \to 0 ; \qquad cdu_1 \to 0 \tag{2.27}$$

$$tnu_1 \to a/\lambda^{\frac{1}{2}} ; \qquad u_1 \to K(k) ; \quad x \to a\cos\phi ; \qquad y \to b\sin\phi$$

In these expressions Φ is given by

$$\Phi = a^2\sin^2\phi + b^2\cos^2\phi \tag{2.28}$$

and K(k) is the complete elliptic integral of the first kind. Upon substituting (2.27) into (2.23) through (2.25) and retaining only those terms containing $(2r)^{-\frac{1}{2}}$ the stresses are found to be

$$\frac{1}{2G}\tau_{zx} = 16a_{10}\sqrt{\frac{\Phi^{\frac{1}{2}}}{2br}}\left(-(1-\eta)\frac{a^{\frac{1}{2}}}{a^4k'}\cos\phi - \eta\frac{b}{a^{5/2}\Phi}\cos^3\phi\right)$$

$$\frac{1}{2G}\tau_{zy} = -16a_{10}\sqrt{\frac{\Phi^{\frac{1}{2}}}{2br}}\left(\frac{\eta}{a^{3/2}\Phi}\sin\phi\cos^2\phi\right) \tag{2.29}$$

The stress components τ_{zn} and τ_{zt} are now found from a stress transformation to be

$$\tau_{zn} = \tau_{zx}\cos\beta + \tau_{zy}\sin\beta$$

$$\tau_{zt} = -\tau_{zx}\sin\beta + \tau_{zy}\cos\beta \tag{2.30}$$

The angle β is related to the parametric equations of an ellipse by

$$\sin\beta = \frac{a\sin\phi}{\Phi^{\frac{1}{2}}}$$

$$\cos\beta = \frac{b\cos\phi}{\Phi^{\frac{1}{2}}} \tag{2.31}$$

Substitution of (2.31) into (2.30) yields the following equations for τ_{zn} and τ_{zt}.

$$\tau_{zn} = \tau_{zx} \frac{b \cos\phi}{\phi^{\frac{1}{2}}} + \tau_{zy} \frac{a \sin\phi}{\phi^{\frac{1}{2}}}$$
$$\tau_{zt} = -\tau_{zx} \frac{a \sin\phi}{\phi^{\frac{1}{2}}} + \tau_{zy} \frac{b \cos\phi}{\phi^{\frac{1}{2}}} \qquad (2.32)$$

Substituting (2.29) into (2.32) and the results of this into (2.17) yields:

$$K_2 = \frac{-32G\pi^{\frac{1}{2}}}{(ab)^{3/2}} \phi^{-\frac{1}{4}} \left(\frac{b}{a}\right) a_{10} \cos^2\phi \qquad (2.33)$$

$$K_3 = \frac{32G\pi^{\frac{1}{2}}(1-\nu)}{(ab)^{3/2}} \phi^{-\frac{1}{4}} a_{10} \sin\phi \cos\phi \qquad (2.34)$$

Similar calculations have been done for every term a_{mn} and b_{mn}. The resulting equations are presented in Appendix II.

Chapter 3

THE HALF-SPACE PROBLEM

1.0 Discussion of the Method

This solution, which was referred to earlier as "Solution 2", gives the stresses in a half-space subjected to uniform normal and shear tractions over a rectangular portion of the surface of the half-space. The general formulation for this problem was originally developed by Boussinesq and Cerruti (23) for the cases in which the rectangular area is subjected to surface tractions normal and parallel to the surface of the half-space. Love (24) worked the problem in detail for the case in which the rectangular area is subjected to uniform normal stress. Alavi (11) gave the solution for the case where the rectangular area is subjected to shear tractions.

Love's solution (24) gave the six stress components caused by the application of a load normal to the plane. Two of these components, $\widehat{yx}$ and $\widehat{yz}$ in Love's notation are needed for Solution 2. However, no derivation for these two components existed for the cases in which the two shearing components of the traction vector were applied, so it was necessary to derive these equations.

The equations for the x, y, and z displacements are presented by Love (23) as:

$$u = \frac{1}{2\pi\mu}\left[\frac{\partial F}{\partial z} - \frac{1}{2}\frac{\partial H}{\partial x} + \frac{\lambda}{2(\lambda+\mu)}\frac{\partial \psi_1}{\partial x} - \frac{1}{2}z\frac{\partial \psi}{\partial x}\right] \tag{3.1}$$

$$v = \frac{1}{2\pi\mu}\left[\frac{\partial G}{\partial z} - \frac{1}{2}\frac{\partial H}{\partial y} + \frac{\lambda}{2(\lambda+\mu)}\frac{\partial \psi_1}{\partial y} - \frac{1}{2}z\frac{\partial \psi}{\partial y}\right] \tag{3.2}$$

$$w = \frac{1}{2\pi\mu}\left[\frac{1}{2}\frac{\partial H}{\partial z} + \frac{1}{2}\frac{\mu}{(\lambda+\mu)}\psi - \frac{1}{2}z\frac{\partial \psi}{\partial z}\right] \tag{3.3}$$

where λ and μ are Lame's constants defined as

$$\lambda = \frac{E\eta}{(1+\eta)(1-2\eta)}$$

μ = shear modulus

and

E = modulus of elasticity

η = Poisson's ratio

The harmonic functions F, G, H, ψ, and ψ_1, are defined in Love (23), and Smith and Alavi (12), and will not be further defined here since this solution may be explained with no additional knowledge of them.

Equations (3.1), (3.2), and (3.3) are written in terms of what shall hereafter be called Love's coordinate system, which is different from the one used in Chapters 1 and 2. This coordinate system is used in Figs. 6 and 7 where it may be seen that in terms of Love's coordinates the desired shear stresses on the surface of the crack are τ_{yx} and τ_{yz}. Love's notation will also be used to specify which component of the surface traction vector is being considered. In this notation, X_v, Y_v, and Z_v represent the applied load at the center of each rectangle in the x, y, and z directions, respectively. The derivations involving these components will be considered separately, and the overall solution will be obtained by superimposing the results from each.

2.0 Derivation of Stresses on the Crack Surface

The strain-displacement equations can be applied to (3.1), (3.2), and (3.3) to provide equations for the strains. Then the stress-strain relations can be used to yield equations for the desired stress components, τ_{yx} and τ_{yz}. These steps are accomplished in the next three

sections for the application of X_ν, Y_ν, and Z_ν to a typical rectangular area in the first quadrant of the plane.

2.1 Stress Derivations when Applying X_ν

Figure 6 shows the coordinate system for a typical rectangle used in this half-space solution. A shearing traction vector X_ν is applied parallel to the x-axis on the surface of the rectangle. This is described by the following boundary conditions.

$$\tau_{zx} = -X_\nu \quad (|x| < a,\ |y| < b,\ z = 0)$$
$$\sigma_{xx} = \sigma_{xy} = \sigma_{zz} = \tau_{xy} = \tau_{zy} = 0 \quad (|x| > a \text{ or } |y| > b) \tag{3.4}$$

Calculations made for τ_{yx} using the steps mentioned in the previous section yield:

$$\tau_{yx} = \frac{1}{2\pi}\left[\frac{\partial^2 F}{\partial y \partial z} + \frac{\lambda}{(\lambda+\mu)}\frac{\partial^2 \psi_1}{\partial x \partial y} - z\frac{\partial^2 \psi}{\partial x \partial y}\right] \tag{3.5}$$

where

$$\frac{\partial^2 F}{\partial y \partial z} = X_\nu \log\left[\frac{d_4+(a-x)}{a_1+(a-x)}\right]\left[\frac{b_2-(a+x)}{c_3-(a+x)}\right] \tag{3.6}$$

$$\frac{\partial^2 \psi}{\partial x \partial y} = X_\nu\left[-\frac{a-x}{a_1(z+a_1)} - \frac{a+x}{b_2(z+b_2)} + \frac{a+x}{c_3(z+c_3)} + \frac{a-x}{d_4(z+d_4)}\right] \tag{3.7}$$

$$\frac{\partial^2 \psi_1}{\partial x \partial y} = z\frac{\partial^2 \psi}{\partial x \partial y} + X_\nu\left[\frac{a-x}{a_1} + \frac{a+x}{b_2} - \frac{a+x}{c_3} - \frac{a-x}{d_4}\right] \tag{3.8}$$

The terms a_1, b_2, c_3, and d_4 are defined as

$$a_1 = \left[(a-x)^2 + (b-y)^2 + z^2\right]^{1/2}$$
$$b_2 = \left[(a+x)^2 + (b-y)^2 + z^2\right]^{1/2}$$

$$c_3 = \left[(a+x)^2 + (b+y)^2 + z^2\right]^{\frac{1}{2}}$$

$$d_4 = \left[(a-x)^2 + (b+y)^2 + z^2\right]^{\frac{1}{2}}$$

Similar calculations made for the other shear component on the surface of the crack give

$$\tau_{yz} = \frac{1}{2\pi}\left[-z\,\frac{\partial^2\psi}{\partial y\partial z}\right] \tag{3.9}$$

where

$$\frac{\partial^2\psi}{\partial y\partial z} = X_\nu\left[\frac{1}{a_1} - \frac{1}{b_2} + \frac{1}{c_3} - \frac{1}{d_4}\right] \tag{3.10}$$

2.2 Stress Derivations when Applying Y_ν

A shearing traction vector Y_ν is applied parallel to the y-axis, with the following boundary conditions:

$$\tau_{zy} = -Y_\nu \quad (|x| < a,\ |y| < b,\ z = 0)$$

$$\sigma_{xx} = \sigma_{yy} = \sigma_{zz} = \tau_{xy} = \tau_{zx} = 0, \quad (|x| > a \text{ or } |y| > b) \tag{3.11}$$

The following equation for τ_{yx} is obtained:

$$\tau_{yx} = \frac{1}{2\pi}\left[\frac{\partial^2 G}{\partial x\partial z} + \frac{\lambda}{(\lambda+\mu)}\,\frac{\partial^2\psi_1}{\partial x\partial y} - z\,\frac{\partial^2\psi}{\partial x\partial y}\right] \tag{3.12}$$

where the derivatives were found to be

$$\frac{\partial^2 G}{\partial x\partial z} = Y_\nu \log\frac{\left[d_4-(b+y)\right]\left[b_2+(b-y)\right]}{\left[a_1+(b-y)\right]\left[c_3-(b+y)\right]} \tag{3.13}$$

$$\frac{\partial^2\psi}{\partial x\partial y} = Y_\nu\left[-\frac{b-y}{a_1(z+a_1)} + \frac{b-y}{b_2(z+b_2)} + \frac{b+y}{c_3(z+c_3)} - \frac{b+y}{d_4(z+d_4)}\right] \tag{3.14}$$

$$\frac{\partial^2\psi_1}{\partial x\partial y} = z\,\frac{\partial^2\psi}{\partial x\partial y} + Y_\nu\left[\frac{b-y}{a_1} - \frac{b-y}{b_2} - \frac{b+y}{c_3} + \frac{b+y}{d_4}\right] \tag{3.15}$$

Calculations made for τ_{yz} give

$$\tau_{yz} = \frac{1}{2\pi}\left[\frac{\partial^2 G}{\partial z^2} - z\frac{\partial^2 \psi}{\partial y \partial z}\right] \tag{3.16}$$

where

$$\frac{\partial^2 \psi}{\partial y \partial z} = -\gamma_\nu\left[\frac{b-y}{(b-y)^2+z^2}\left(\frac{a-x}{a_1}+\frac{a+x}{b_2}\right)+\frac{b+y}{(b+y)^2+z^2}\left(\frac{a-x}{d_4}+\frac{a+x}{c_3}\right)\right] \tag{3.17}$$

G is a harmonic function, so

$$\frac{\partial^2 G}{\partial z^2} = -\left(\frac{\partial^2 G}{\partial x^2}+\frac{\partial^2 G}{\partial y^2}\right) \tag{3.18}$$

$$\frac{\partial^2 G}{\partial x^2} = \gamma_\nu\left[\tan^{-1}\frac{b-y}{a-x}+\tan^{-1}\frac{b+y}{a-x}-\tan^{-1}\frac{z(b-y)}{(a-x)a_1}-\tan^{-1}\frac{z(b+y)}{(a-x)d_4}+\right.$$
$$\left.+\tan^{-1}\frac{b-y}{a+x}+\tan^{-1}\frac{b+y}{a+x}-\tan^{-1}\frac{z(b-y)}{(a+x)b_2}-\tan^{-1}\frac{z(b+y)}{(a+x)c_3}\right] \tag{3.19}$$

$$\frac{\partial^2 G}{\partial y^2} = \gamma_\nu\left[\tan^{-1}\frac{a-x}{b-y}+\tan^{-1}\frac{a+x}{b-y}-\tan^{-1}\frac{z(a-x)}{(b-y)a_1}-\tan^{-1}\frac{z(a+x)}{(b-y)b_2}+\right.$$
$$\left.+\tan^{-1}\frac{a-x}{b+y}+\tan^{-1}\frac{a+x}{b+y}-\tan^{-1}\frac{z(a-x)}{(b+y)d_4}-\tan^{-1}\frac{z(a+x)}{(b+y)c_3}\right] \tag{3.20}$$

2.3 Stress Derivations when Applying Z_ν

The normal traction vector z_ν is applied parallel to the z-axis and perpendicular to the plane, providing the following boundary conditions:

$$\sigma_{zz} = -z_\nu \quad (|x| < a,\ |y| < b,\ z = 0)$$
$$\sigma_{xx} = \sigma_{yy} = \tau_{xy} = \tau_{zx} = \tau_{zy} = 0 \quad (|x| > a \text{ or } |y| > b) \tag{3.21}$$

Calculations made for τ_{yx} yield

$$\tau_{yx} = \frac{-1}{2\pi} \left[\frac{\mu}{(\lambda+\mu)} \frac{\partial^2 H}{\partial x \partial y} + z \frac{\partial^2 \psi}{\partial x \partial y} \right] \tag{3.22}$$

where

$$\frac{\partial^2 H}{\partial x \partial y} = Z_v \log \frac{(z+a_1)(z+c_3)}{(z+b_2)(z+d_4)} \tag{3.23}$$

$$\frac{\partial^2 \psi}{\partial x \partial y} = Z_v \left[\frac{1}{a_1} - \frac{1}{b_2} + \frac{1}{c_3} - \frac{1}{d_4} \right] \tag{3.24}$$

The following equation is obtained for τ_{yz}

$$\tau_{yz} = \frac{1}{2\pi} \left[-z \frac{\partial^2 \psi}{\partial y \partial z} \right] \tag{3.25}$$

where

$$\frac{\partial^2 \psi}{\partial y \partial z} = Z_v \left[\frac{z}{(b-y)^2+z^2} \left(\frac{a-x}{a_1} + \frac{a+x}{b_2} \right) - \frac{z}{(b+y)^2+z^2} \left(\frac{a-x}{d_4} + \frac{a+x}{c_3} \right) \right] \tag{3.26}$$

3.0 The Solution Form for Application to the Crack Problem

When using the half-space solution, each quadrant of the plane is divided into a number of small rectangles, as shown in Fig. 2. The exact number of rectangles used can vary, depending upon the particular crack shape a/2c, and the amount of crack penetration into the plate, a/t. The effect of applying the normal and shear loading to each rectangle must be considered when the stress at any particular point is calculated. The number of calculations would tend to get out of hand if a large number of rectangles were used, so it is desirable to take advantage of the symmetry conditions of the stresses and thus reduce the

number of total calculations necessary. Therefore, calculations are made using only the rectangles in one quadrant of the surface.

The principle of superposition is used to determine the shear stresses on the face of the crack, τ_{yx} and τ_{yz}, by adding the effects of applying X_ν, Y_ν, and Z_ν. In order to clarify the procedure, and shorten the length of the equations used, the following shorthand notation will be adopted. Let (3.5), (3.12), and (3.22) be called F1X, F2X, and F3X, respectively. The number 1, 2, or 3 identifies with the direction of loading, X_ν, Y_ν, or Z_ν, respectively, while the last letter X identifies that the shear component in the x-direction, τ_{yx}, is being determined. In a like manner, let (3.9), (3.16), and (3.25) be identified as F1Z, F2Z, and F3Z, respectively, where the Z denotes that the stress component in the z-direction, τ_{yz} is being considered.

Using superposition, and factoring the applied load from each of the equations mentioned above, the τ_{yx} component may be written:

$$\tau_{yx} = X_\nu \, F1X + Y_\nu \, F2X + Z_\nu \, F3X \tag{3.27}$$

Consider the case in which a uniform load is applied to the surface of the crack in the x-direction only. This would correspond to the loading being applied in the direction of τ_{yx} as shown in Fig. 7, and would result in the stress symmetries on the surface of the plane as shown in the same figure. These symmetries may be written as

$$\begin{aligned} \tau_{zx} &= -Y_\nu = \text{Even in X, Odd in Y} \\ \tau_{zy} &= -Y_\nu = \text{Odd in X, Even in Y} \\ \sigma_{zz} &= -Z_\nu = \text{Odd in X, Odd in Y} \end{aligned} \tag{3.28}$$

They will be used in generalizing the solution for computer use.

A check of the symmetries of the equations derived for F1X, F2X, and F3X, shows them to be:

$$\begin{aligned} &F1X = \text{Even in X, Odd in Y} \\ &F2X = \text{Odd in X, Even in Y} \\ &F3X = \text{Odd in X, Odd in Y} \end{aligned} \tag{3.29}$$

To illustrate how these symmetries are used, consider only the effect of the X_ν surface traction on four rectangular areas, located symmetrically in each of the four quadrants, as shown in Fig. 7. Then

$$\begin{aligned} F1X_1 &= F1X\ (X - \bar{X},\ Y - \bar{Y},\ Z), && \text{first quadrant} \\ F1X_2 &= F1X\ (X + \bar{X},\ Y - \bar{Y},\ Z), && \text{second quadrant} \\ F1X_3 &= F1X\ (X - \bar{X},\ Y + \bar{Y},\ Z), && \text{third quadrant} \\ F1X_4 &= F1X\ (X + \bar{X},\ Y + \bar{Y},\ Z), && \text{fourth quadrant} \end{aligned} \tag{3.30}$$

where X, Y, and Z are the coordinates of the point at which the stresses are being calculated, while $\bar{X}$ and $\bar{Y}$ are the coordinates of the center of the rectangle being considered. Since the plane is the origin of the coordinate system, the $\bar{Z}$ coordinate is equal to zero. On the plane of the crack, Y = 0, and after using $-\bar{Y}$ and the symmetry conditions of (3.29), equations (3.30) become:

$$\begin{aligned} F1X_1 &= F1X\ (X - \bar{X},\ -\bar{Y},\ Z) \\ F1X_2 &= F1X\ (X + \bar{X},\ -\bar{Y},\ Z) \\ F1X_3 &= -F1X\ (X - \bar{X},\ -\bar{Y},\ Z) \\ F1X_4 &= -F1X\ (X + \bar{X},\ -\bar{Y},\ Z) \end{aligned} \tag{3.31}$$

From (3.31), $F1X_1 = -F1X_3$ and $F1X_2 = -F1X_4$.

Let

$$\tau_{yx} = X_{\nu_1} F1X_1 + X_{\nu_2} F1X_2 + X_{\nu_3} F1X_3 + X_{\nu_4} F1X_4 \tag{3.32}$$

where the subscripts on X_ν indicate the quadrant number. Using the symmetries of (3.28),

$$X_{\nu_1} = X_{\nu_2} = -X_{\nu_3} = -X_{\nu_4} , \tag{3.33}$$

and substituting,

$$\tau_{yx} = 2\, X_{\nu_1} \left[FIX(X-\bar{X},\ -\bar{Y},\ Z) + FIX(X+\bar{X},\ -\bar{Y},\ Z) \right] \tag{3.34}$$

If a similar procedure is followed when applying Y_ν and Z_ν, and if the results from all rectangles are summed, the stress τ_{yx} generated at a point on the surface of the crack is

$$\begin{aligned} \tau_{yx} = &+ \sum_{k=1}^{N} 2\, X_{\nu_k} \left[F1X(X-\bar{X}_k,\ -\bar{Y}_k,\ Z) + F1X(X+\bar{X}_k,\ -\bar{Y}_k,\ Z) \right] + \\ &+ \sum_{k=1}^{N} 2\, Y_{\nu_k} \left[F2X(X-\bar{X}_k,\ -\bar{Y}_k,\ Z) - F2X(X+\bar{X}_k,\ -\bar{Y}_k,\ Z) \right] + \\ &+ \sum_{k=1}^{N} 2\, Z_{\nu_k} \left[F3X(X-\bar{X}_k,\ -\bar{Y}_k,\ Z) - F3X(X+\bar{X}_k,\ -\bar{Y}_k,\ Z) \right] \end{aligned} \tag{3.35}$$

where k is a particular rectangle number and N is the total number of rectangles in the first quadrant.

In the same manner as above, the τ_{yz} component of the stress may be written as:

$$\tau_{yz} = X_\nu\, F1Z + Y_\nu\, F2Z + Z_\nu\, F3Z \tag{3.36}$$

The equations for F1Z, F2Z, and F3Z provide the following symmetries:

$$\begin{aligned} &F1Z = \text{Odd in X, Odd in Y} \\ &F2Z = \text{Even in X, Even in Y} \\ &F3Z = \text{Even in X, Odd in Y} \end{aligned} \tag{3.37}$$

If the same procedure is followed to calculate τ_{yz} as was followed to calculate τ_{yx} in (3.35), the results will be:

$$\tau_{yz} = + \sum_{k=1}^{N} 2\, X_{\nu_k} \left[F1Z(X-\bar{X}_k,\ -\bar{Y}_k,\ Z) + F1Z(X+\bar{X}_k,\ -\bar{Y}_k,\ Z) \right] +$$

$$+ \sum_{k=1}^{N} 2\, Y_{\nu_k} \left[F2Z(X-\bar{X}_k,\ -\bar{Y}_k,\ Z) - F2Z(X+\bar{X}_k,\ -\bar{Y}_k,\ Z) \right] + \quad (3.38)$$

$$+ \sum_{k=1}^{N} 2\, Z_{\nu_k} \left[F3Z(X-\bar{X}_k,\ -\bar{Y}_k,\ Z) - F3Z(X+\bar{X}_k,\ -\bar{Y}_k,\ Z) \right]$$

Chapter 4

THE COMPUTER PROGRAM

1.0 General Makeup of the Program

The mathematical derivations discussed in Chapters 2 and 3 result in an appalling number of equations which must be solved to provide a solution to the problem. Additionally, the alternating technique with its iterations causes many of these equations to be solved repeatedly during the solution procedure used for a single crack geometry. The magnitude of the problem dictates that the digital computer be utilized to obtain the solutions. Therefore, the entire problem was programmed into the Fortran IV language to be used on the Colorado State University CDC 6400 computer.

Subroutines were used to a great extent in the makeup of the program. Generally, a separate subroutine was written to accomplish each individual portion of the overall solution. The subroutines were then called in the proper sequence necessary to successfully achieve the solution to the problem.

As each subroutine which performed a particular function was written, it was checked and debugged individually or in conjunction with some other required subroutines. This facilitated the checkout of the large program when the subroutines were added to it since they had already been checked to be operational on an individual basis. After an initial period of debugging, the proven portions of the large program were put on permanent file in the computer. Five individual cycles of a single file name were used so that any changes in a particular subroutine would necessitate changes only to one cycle, which constituted only a small portion of the total.

The following steps in abbreviated form show the operating sequence of the computer program.

1. Read the input data for the problem being solved. This data includes input loading in terms of coefficients A_{mn} and B_{mn}, crack and plate geometries, number of cycle iterations to be made, and the dimensional information for the rectangular grids used on both the front and back surfaces.
2. Generate the coordinates for the 96 points on the crack surface for which stress calculations are to be made.
3. Generate the initial shear stress loading on each of the points on the crack surface from the input coefficients A_{mn} and B_{mn}.
4. Perform a least squares fit of the stress distribution calculated in the last step. This step is not necessary when the stress distribution being fitted is the initial loading determined by the coefficients prescribed in step one, but it is done for this first iteration to keep the program general enough to handle successive iterations, and also as a check on the accuracy of the least squares solution for a known loading case. The method of least squares is discussed in more detail in Section 2.2.
5. Calculate the modulus and complementary modulus of the Jacobian elliptic functions and integrals, and compute the complete elliptic integrals of the first and second kinds. All four of these functions are used in the 20 x 20 K_{ij} matrix of equation (2.16).
6. Using the functions of the last step, determine the nonzero terms of the K_{ij} matrix. Use a Gauss elimination method to

solve the matrix equation, and calculate the coefficients a_{mn} and b_{mn}.

7. Calculate the mode two and mode three stress intensity factors, K_2 and K_3. Nondimensionalize these factors and call them M_2 and M_3, the stress intensity magnification factors.
8. Calculate the stresses at the center of each rectangle on the front surface. This requires the following steps for each rectangle:
   8.1 Calculate the ellipsoidal coordinates λ, μ and ν of the rectangle center.
   8.2 Calculate the required elliptic integrals, Jacobian elliptic functions, and partial derivatives. Compute the stresses at the center of each rectangle.
9. Calculate the stresses on the crack due to freeing the stresses on the front surface.
10. Perform steps four through seven for the new loading on the crack surface. Repeat steps eight through ten for as many iterations as are desired on the front surface.
11. Obtain the total stress applied to the front surface and use this total to calculate the resulting residual stresses at the center of each rectangle of the grid on the back surface, as in 8.1 and 8.2.
12. Calculate the stresses on the crack due to freeing the stresses on the back surface.
13. Repeat steps four through seven for the new loading on the crack surface.

14. Obtain the total stresses applied to the crack in steps three and nine, and repeat steps four through 14 for the back surface. This completes one cycle of iteration, and should be repeated until the stress intensity factors are negligible compared to the ones obtained from the original applied load.

2.0 Special Subroutines Used

Some of the subroutines used in Section 1.0 should be discussed to point out details of their operation.

2.1 Crack Coordinate Generator

A subroutine called COORD is used to generate the 96 points on the crack surface for which stress calculations are to be made. Considerations of symmetry enable calculations to be made on only the half of the crack for which x is positive, as shown in Fig. 3.

The coordinate generator uses five similar ellipses, each with a semiminor and semimajor axis which is a particular fraction of the length of the axes of the outer ellipse. The ratios used in this case were 0.2, 0.4, 0.6, 0.8, and 1.0. Coordinates were generated by a simultaneous solution of the two equations

$$\frac{x^2}{a^2} + \frac{y^2}{b^2} = 1 \tag{4.1}$$

and

$$\tan \phi = y/x \tag{4.2}$$

where the angle ϕ was increased in 10 degree increments for each of the five similar ellipses. Values were calculated only in the first quadrant (positive x and y) and then reflected with the proper sign into the other quadrant.

2.2 Least Squares Curve Fitting

The loading on the crack surface for which all calculations were made in this work was one in which only a uniform x-component τ_{zx} was applied as shown in Fig. 4. A consideration of the problem shows that the τ_{zx} and τ_{zy} components applied back on the crack surface through the iteration process have symmetries which state that τ_{zx} is even in x and τ_{zy} is odd in x. Because of these symmetries, the least squares curve fitting process is slightly different for each of these two components.

If τ_{zx} is even in x, the first of equations (2.3) becomes:

$$\tau_{zx} = A_{00} + A_{01}\, y + A_{20}\, x^2 + A_{02}\, y^2 + A_{21}\, x^2 y + A_{03}\, y^3 \tag{4.3}$$

The τ_{zx} stress components calculated at the 96 points mentioned in the last section are used in the least squares subroutine, LEAST, which calculates the fit for this component.

The component τ_{zy} is odd in x, so the last of equations (2.3) may be written:

$$\tau_{zy} = B_{00} + B_{10}\, x + B_{11}\, xy + B_{02}\, y^2 + B_{12}\, xy^2 + B_{30}\, x^3 \tag{4.4}$$

After the τ_{zy} components were calculated on the surface of the crack the method of least squares was used on the stress distribution to calculate the B_{mn} coefficients in a subroutine called LEAST2.

The least squares criterion used is a general one in which

$$E = \sum_{i=1}^{N} \left[P(x_i, y_i) - f(x_i, y_i) \right]^2 \tag{4.5}$$

where

$P(x_i, y_i)$ = tabular pressure values

$f(x_i, y_i)$ = family of functions representing the pressure, which in this case would be (4.3) or (4.4).

The best fit will be obtained if E is a minimum. This is obtained by setting

$$\frac{\partial E}{\partial A_{mn}} = 0 \tag{4.6}$$

where A_{mn} represents the coefficients in (4.3) or (4.4).

2.3 Calculation of Elliptic Integrals

The complete elliptic integrals of the first and second kinds are required in the elements of the K_{ij} matrix in equation (2.16), so they must be evaluated for their use there. A polynomial approximation, as presented in Abramowitz and Stegun (27), is used to calculate the values of these integrals. The absolute value of the error associated with these polynomials is no greater than 2.0×10^{-8}, so it is sufficiently accurate for the intended purpose.

Incomplete elliptic integrals of the first and second kinds are required for the stress calculations of Solution 1. These integrals are evaluated using the process of the arithmetic-geometric mean, which is also presented in (27).

2.4 Ellipsoidal Coordinates

Ellipsoidal coordinates λ, μ and ν were obtained as the roots of the cubic equation (2.8). The Newton-Raphson method was used to find the first root, and the quadratic equation solution was then used to find the other two roots of the reduced polynomial. The three roots thus determined were placed in the order of ascending magnitude and each was matched with its proper ellipsoidal coordinate, as shown in (2.10). A final check was made to assure that the coordinates did indeed have the proper relative magnitudes of (2.10), and could satisfy the transformation equations (2.9).

3.0 Rectangular Surface Grids

A typical rectangular surface grid used to calculate and remove stresses from the front and back surfaces is shown in Fig. 2. Most of the cases run utilized a grid with 62 rectangles on the front surface and a grid with 32 rectangles on the back surface. However, more rectangles were used in cases involving thin cracks or cracks which penetrated the plate for a major part of the thickness. The total computer time used is dramatically affected by the number of rectangles on each surface, so the number was kept to a minimum consistent with the desired accuracy and convergence required for each particular crack geometry.

Chapter 5

DISCUSSION OF RESULTS FOR PART I

The results included in this section were obtained from computer calculations using the equations developed in the previous chapters. All results shown are for the loading case in which a uniform shear load τ_{zx} was applied to the surface of the crack, parallel to the x-axis, as shown in Fig. 4. The initial loading did not include the application of the shear component in the y-direction, τ_{zy}. This particular initial loading reduces the first of equations (2.3) to the case where all A_{mn} coefficients except A_{00} are equal to zero, while all coefficients of the second equation of (2.3) are equal to zero. Solutions 1 and 2 of the previous chapters were used with the alternating method to determine the mode two and mode three stress intensity factors for a semielliptical surface crack in the surface of a finite thickness solid.

1.0 Results and Discussion

Mode two and mode three stress intensity factors were calculated for several semielliptical surface crack shapes subjected to uniform shear loading applied only in the x-direction. The various crack shapes considered had a/2c ratios of 0.05, 0.1, 0.2, 0.3, and 0.4, and had depth ratios a/t varying from 0.2 to 0.9. A Poisson's ratio of 0.25 was used for all calculations.

Figures 9 through 13 present the mode two and mode three stress intensity factors as a function of the parametric angle ϕ which is measured from the semiminor axis of the ellipse, as shown in Fig. 8. The stress intensity factors K_2 and K_3 have been nondimensionalized and plotted as M_2 and M_3, respectively, where

$$M_2 = \frac{K_2}{\tau_{zx}(\pi a/Q)^{\frac{1}{2}}} \tag{5.1}$$

and

$$M_3 = \frac{K_3}{\tau_{zx}(\pi a/Q)^{\frac{1}{2}}} \tag{5.2}$$

The stress τ_{zx} is the initially applied loading, "a" is the semiminor axis, and $Q^{\frac{1}{2}} = E(k)$, the complete elliptic integral of the second kind.

The process of iterating between the crack and the front and back surfaces of the plate causes the K_2 and K_3 curves to assume new shapes and values as compared to those obtained for the embedded crack. Several effects interact to influence the variation of the shape of these curves, and an inspection of the step-by-step output from the computer analysis reveals the following trends:

1. The crack shape effect: This effect is a result of the elliptical crack solution. It causes K_2 to increase and K_3 to decrease as the angle ϕ varies from 0 to 90 degrees. The range through K_2 increases becomes smaller as the crack shape goes from a/2c = 0.40 to 0.05, while the range through which K_3 decreases becomes larger with the same variation in crack shape.
2. The front surface effect: This effect increases the value of K_3 as the angle ϕ varies from 0 to 90 degrees, and is larger for cracks having large a/2c ratios than it is for the slender cracks having small a/2c ratios. It is this effect which produces a small value for K_3 at $\phi = 90^{\circ}$ on cracks having a/2c = 0.20 and larger.

3. The back surface effect: This increases the value of K_3 by an amount which is maximum at $\phi = 0°$. As ϕ is allowed to range from 0 to 90 degrees the increase in K_3 diminishes and essentially disappears at about 60 or 70 degrees. This back surface effect also causes K_2 to increase from zero at $\phi = 0°$ to a maximum at approximately 40 or 50 degrees, and drop back to a minimum value at $\phi = 90°$. The magnitude of change in K_2 is substantially less than that in K_3, especially for a/t ratios greater than 0.5, where the magnitude of K_3 is substantial.
4. Effect of the interaction between the front and back surfaces: This effect causes both K_2 and K_3 to increase. The increase of K_2 becomes greater as ϕ varies from 0 to 90 degrees, while the increase of K_3 becomes smaller as ϕ ranges from 0 to 90 degrees.

It should be noted that the K_3 curves in the figures are all concave downward, while the K_2 curves are concave downward for the larger values of a/2c and concave upward for a/2c values less than 0.2. The results of this study, and those of Kassir and Sih (22) show that for an ellipse embedded in an infinite solid with only the τ_{zx} component applied, the curvature of the K_2 plot changes sign at an a/2c value of approximately 0.2. The behavior is a result of the crack shape effect for the particular loading used.

Figures 9 through 13 show that the values for K_3 at $\phi = 0$ degrees increase with larger depth ratios a/t. This is due primarily to the back surface effect which exerts its maximum influence at $\phi = 0°$. This

effect becomes increasingly important as the crack nears the back surface with large a/t ratios.

The figures will show that cracks with higher a/t ratios exhibit greater K_2 values than do those with lower a/t values. This is true for every value of ϕ except 0 degrees where K_2 for all cracks is zero. These increases with higher a/t values can be attributed to the back surface effect, and the effects of the interaction between the front and back surfaces.

All depth ratios a/t provide a value of zero for K_2 at $\phi = 0^o$. According to equation (2.17) K_2 can exist only if the stress component τ_{zn} exists at this point. At the angle $\phi = 0^o$ the tip of the crack is perpendicular to the y-axis, so the τ_{zn} component in this case is τ_{zy} which is an odd function of x. Since $x = 0$ at $\phi = 0^o$, then τ_{zy} must also be zero at this point, and K_2 must be the same. This justifies the fact that K_2 at $\phi = 0^o$ is always zero, and also provides a check on the computer results for that point.

Figures 9 through 13 show that the stress intensity factors approach a finite value at the angle $\phi = 90^o$. It is felt, however, that the curves may not represent the true behavior of the elastic solution where the crack tip intersects the surface of the plate because it is expected that there is a change in the nature of the crack tip singularity at that point. Hartranft and Sih (28) used a refined numerical analysis to study the problem of a semicircular surface crack subjected to normal loading. Their analysis utilized a very large number of surface rectangles and terms in the mathematical expressions used to calculate the stresses, and considered the singular and nonsingular portions of the surface stresses separately. They noted that the stress

intensity factor for the problem which they solved would tend to approach zero at the surface, though they were unable to extend the calculation to the point of intersection. Smith (29) concluded that the results obtained by Smith (8) and Thresher (14) agree well with those of Hartranft and Sih over most of the crack front although the smaller number of rectangles and mathematical terms used by Smith and Thresher miss the effect of the decrease in the stress intensity factor near $\phi = 90^{o}$.

It is expected that a comparable uncertainty exists in the behavior at the surface of the plate for the shear problem. The analytical approach used in this study, however, should be accurate along most of the crack front. The value of the stress intensity factors shown in the curves is representative of the average near $\phi = 90^{o}$.

The cost of the computer time necessary to perform a refined analysis such as the one by Hartranft and Sih becomes prohibitive. A serious study becomes necessary in which the advantages of greater accuracy are considered and weighed against the increased computer costs incurred.

Figure 14 presents the values of maximum K_2 plotted against depth ratios a/t for cracks with a/2c values of 0.05, 0.1, 0.2, 0.3, and 0.4. It should be noted that the curve for a particular crack shape increases gently and smoothly as the depth ratio increases. There is a sizeable difference in the K_2 values for slender cracks with a/2c = 0.05 as compared with thicker cracks with a/2c values of 0.4.

The maximum value of K_2 plotted in Fig. 14 is determined at $\phi = 90^{o}$ from Figs. 9 through 13. Considerations advanced in preceding paragraphs indicate that the maximum true value for K_2 may not exist at

$\phi = 90°$, but this value is representative of K_2 in an average sense near $\phi = 90°$.

Values of K_3 for cracks with a/2c values ranging from 0.05 to 0.4 are plotted against depth ratios a/t in Fig. 15. It should be noted that these curves for the corresponding range of a/2c values are clustered closer together than are those for K_2. These K_3 curves also rise quite rapidly as the a/t ratio is increased beyond approximately 0.6. This trend was not noticed with the K_2 curves, and indicates that cracks of this type are quite mode three sensitive to crack depth ratios.

The results reveal that there is only a slight change in the maximum K_2 and K_3 values for semielliptical cracks having low a/t ratios of 0.2, compared to the maximum K_2 and K_3 values for embedded ellipses of the same shape. The maximum K_3 value for a crack having an a/2c ratio of 0.2 increased by 15.1 and 31.2 percent as a/t was increased to 0.8 and 0.9, respectively, while the maximum K_2 value increased by 6.0 and 7.1 percent, respectively, under the same conditions. A crack having an a/2c of 0.3 showed an increase in K_3 of 11.2 and 22.6 percent and an increase in K_2 of 5.3 and 6.7 percent as a/t was increased to 0.8 and 0.9, respectively. Similar increases were noted in both K_2 and K_3 for other crack geometries.

2.0 Accuracy and Convergence

Rectangular grids similar to the one illustrated in Fig. 2 were used on the front and back surfaces in the alternating technique employed for this problem. It had previously been determined from other problems that convergence difficulties could exist if the rectangle sizes were too large for the problem geometry being considered. It was

discovered in the shear problem that convergence was not as difficult to attain as in the normal loading problem. The shear problem for a particular geometry could be worked using coarser grids and generally fewer cycles than what were required for the normal problem. Usually a front grid with 62 rectangles, a rear grid with 32 rectangles, and two cycles of iteration were adequate to achieve excellent convergence for most problems. However, it was necessary to use four cycles and finer grids for problems having high a/t ratios, especially for those having low a/2c values.

Figure 16 shows the stress intensity factors after each cycle of iteration for a typical run in which four cycles were made on a crack geometry of a/2c = 0.2 and a/t = 0.9. It should be noted that the value of the stress intensity factors increases for each cycle, and that the contribution of each successive cycle becomes smaller until the last cycle produces essentially an insignificant change. The differences between cycles three and four for K_2 are too small to be plotted on the scale used in the figure.

The following tabulation shows the percentage of change of the maximum values of K_2 and K_3 accomplished by each cycle of iteration.

Cycle	Percent Change in K_2	Percent Change in K_3
1	4.74	24.30
2	1.42	4.09
3	0.57	1.07
4	0.22	0.35

Obviously some truncation error exists in the final results due to stopping the iteration process at a finite number of cycles. However,

enough cycles of iteration were performed in each case to insure that the change in the stress intensity factors which would be obtained by further iterations was of an insignificant magnitude and did not warrant the expenditure of additional computer time.

Accuracy of the solution was checked by making two computer runs each on several cracks, using different surface grids for each of the runs on a specific crack geometry. The results of the runs for a particular crack configuration were then compared to determine the difference which existed between them. Cracks considered in this manner had a/2c values of 0.05 and 0.1, and a/t values of 0.8 and 0.9. Solutions obtained from grids with 62 front and 32 back rectangles were compared with those obtained from grids with 55 front and back rectangles. Changing from one set of grids to the other caused the maximum values of K_2 to differ by 0.1 to 2.0 percent, and the maximum values of K_3 to differ by 0.6 to 0.9 percent.

The results discussed in this chapter are obtained by numerical methods and thus include the step-by-step accumulation of numerical inaccuracies inherent in methods of this type. Although these results cannot be considered as an exact solution to the problem, they represent the best solutions available.

The program was compiled under the Fortran Extended option which would give the minimum running time. It was then cataloged on permanent file to insure that no compiler time was necessary for the data production runs. Typical running time used by the CDC 6400 computer for 62 rectangles on the front and 32 rectangles on the rear was approximately 510 seconds for two cycles of iteration, and approximately 1015 seconds for four cycles. The cases in which 55 rectangles on each surface were used with four cycles required 1300 seconds.

PART II--NORMAL LOADING OF A SEMIELLIPTICAL SURFACE CRACK

Chapter 6

THE NORMAL LOADING PROBLEM

1.0 Statement of the Semielliptical Surface Crack Problem

Consider a flat semielliptical surface crack located in the front surface of a finite thickness slab. The geometrical configuration is the same as that shown in Fig. 1, but there is no shear loading applied to the surface of the crack for this problem. Instead, the surface of the crack is subjected to nonuniform normal stresses σ_{zz}.

The boundary conditions to be considered in the solution of this problem are as follows:

$$\tau_{zx} = \tau_{zy} = 0 , \quad (z = 0) \tag{6.1}$$

and

$$w = 0 , \left(\frac{x^2}{a^2} + \frac{y^2}{b^2} > 1 \; ; \; z = 0 \right) \tag{6.2}$$

where w is the displacement in the z-direction.

It is assumed that the normal stress applied to the surface of the crack is expressible as

$$\sigma_{zz} = \sum_{m=0}^{3} \sum_{n=0}^{3} A_{mn} x^m y^n , \left(\frac{x^2}{a^2} + \frac{y^2}{b^2} \leq 1 \; ; \; z = 0 \right) \tag{6.3}$$

where $m + n \leq 3$ because of the magnitude of work required in the calculations if the sum were allowed to be larger than three. The front and back surfaces of the body are considered to be free of stresses.

2.0 The Method of Solution

The method of solution which will be used for this problem is essentially identical to the one used for the shear problem which has

been discussed in previous chapters. The alternating technique is once again used with Solutions 1 and 2, defined as follows:

Solution 1. The determination of the stresses near an elliptical crack at any point in an infinite solid through which it is desired to pass a plane. The surface of the crack is subjected to nonuniform normal loading.

Solution 2. The determination of the stresses within a half-space subjected to uniform normal and shear stress over a rectangular portion of the surface.

Solutions one and two are discussed briefly in the following two sections.

2.1 Elastic Solution of a Crack in an Infinite Solid

Solution 1 represents the elastic solution of an elliptical crack in an infinite solid subjected to nonuniform normal stresses. The particular form of this solution which was used for this portion of the problem was derived by Shah and Kobayashi (6). Thi method was used by them in an alternating method solution to the problem of an elliptical crack approaching the surface of an semi-infinite solid subjected to uniform tension perpendicular to the plane of the crack (17). Details and the derivations necessary to use the solution may be found in (6, 16, and 17), and will not be repeated here.

2.2 The Half-Space Solution

This solution has previously been identified as "Solution 2", and calculates the stresses in a half-space subjected to uniform normal and shear tractions applied to a rectangular portion of the surface of the half-space. The solution method is similar to that described in Chapter 3, and uses the equations descr ed in (11 and 12).

This portion of Solution 2 calculates only the σ_{zz} component of the stress on the crack surface. The symmetry conditions of the problem prohibit the presence of any residual shear stresses, τ_{zx} or τ_{zy}, on the crack surface. Therefore, no attempt need be made at calculating them since they vanish when all effects from all rectangles are summed.

2.3 The Alternating Method

The alternating method used here is the same as the one used by Thresher and Smith (14, 15), and the method described in Chapter 1 which was used for the shear problem. It differs from the one used for the shear problem in that it calculates only the normal stresses on the crack surface and the resulting mode one stress intensity factor, K_1, while the method described in Chapter 1 calculates both shear stresses on the crack surface and the mode two and mode three stress intensity factors, K_2 and K_3.

As is the case with the shear problem, the alternating method iterations proceed until the change in the mode one stress intensity factor for any one cycle becomes negligible when compared to its value obtained for the initial loading.

3.0 The Computer Program

A computer program was written for the CDC 6400 digital computer which would perform all the calculations for Solutions 1 and 2. The general method of programming was the same as that discussed in Chapter 4 for the shear problem. In fact, the program for the normal loading problem was written before the one for the shear loading problem, and served as the model for it in addition to providing some of the subroutines which are all or partially common to both programs.

The sequence of operations performed and the manner in which the subroutines are used is essentially the same in both programs.

One of the primary differences between the two programs is the much smaller number of equations which must be solved for the normal loading problem. For example, the 20 x 20 K_{ij} matrix of equation (2.16) is only a 10 x 10 matrix for the normal load problem. Since only one component of stress is being applied to the crack instead of two, which is the case with the shear problem, there are only approximately one-half as many terms necessary to calculate the stresses which must be freed from the surfaces of the body.

A study of the symmetries of the normal loading problem reveals that the normal stress on the crack surface σ_{zz} is even in x. This allows (6.3) to be written as

$$\sigma_{zz} = A_{00} + A_{01}\, y + A_{20}\, x^2 + A_{02}\, y^2 + A_{21}\, x^2 y + A_{03}\, y^3 \qquad (6.4)$$

The method of least squares curve fitting is performed on this equation in the same manner as it was performed on the equations for the shear loading problem. After the curve fitting scheme is employed, a matrix equation similar to (2.16), but having a 10 x 10 K_{ij} matrix, is solved for the ten independent a_{mn} coefficients. These in turn are used to calculate the mode one stress intensity factor K_I.

A typical rectangular grid of the type used on the front and back surfaces is shown in Fig. 17, and will be discussed in more detail in the next chapter.

Chapter 7

DISCUSSION OF RESULTS FOR PART II

All computer calculations were run for the case in which a uniform normal load was applied to the surface of the crack. This corresponds to the situation where a uniform tensile load is applied to the body in a direction perpendicular to the plane of the crack. Equation (6.4) is then reduced to the case where all the coefficients A_{mn} in the first iteration step are equal to zero except for A_{00}. Solutions 1 and 2 were used with the alternating method to determine the mode one stress intensity factors for a semielliptical surface crack in the surface of a finite thickness solid.

1.0 Results and Discussion

Four different crack shapes were considered having a/2c ratios of 0.05, 0.10, 0.20, and 0.30, and having depth ratios a/t ranging from 0.20 to 0.95. All computations were made using a Poisson's ratio of 0.25.

The stress intensity factors plotted as a function of the parametric angle ϕ of the ellipse are presented in a nondimensionalized form in Figs. 18 through 21. The angle ϕ is measured from the semiminor axis "a" at the portion of the crack which is farthest into the material, as shown in Fig. 8. Three effects interact to influence the variation of the shape of the stress intensity curves, and are:

1. The effect of the crack shape: This effect is a property of the elliptical crack solution and causes K_1 to decrease as the angle ϕ is varied from 0 to 90 degrees. The value of K_1 is constant for a circular crack with a/2c ratio of 0.5, but

decreases very drastically as ϕ is increased for a slender crack with a/2c = 0.05. Thus the crack shape effect becomes more significant as the crack shape goes from a/2c = 0.5 to a/2c = 0.05.

2. The effect of the front surface: Previous studies (9) and inspection of the present computer solutions show that this effect causes K_1 to increase as ϕ varies from 0 to 90 degrees. The amount of increase from this effect is of smaller magnitude than the crack shape effect.

3. The effect of the back surface: This effect can be considered to include the direct effect of the presence of the back surface as well as the effect of the interaction between the front and back surfaces. The back surface effect alone tends to cause a sharp increase in K_1 near $\phi = 0^\circ$, while the interaction effect between the two surfaces tends to increase K_1 near $\phi = 90^\circ$, but by an amount substantially less than that caused by the back surface effect. The result of the two effects combined is to cause K_1 to increase significantly near $\phi = 0^\circ$ and to increase by a smaller amount near $\phi = 90^\circ$.

The crack shape effect causes a general decrease in K_1 with increasing ϕ, as can be noted in Figs. 18 through 21. The back surface effect causes an increase in K_1 as the thickness ratio a/t is increased. In Figs. 20 and 21, for a/2c of 0.05 and 0.10, an increase in K_1 occurs before the expected decrease begins, which indicates that the maximum value of K_1 does not necessarily occur at $\phi = 0^\circ$. The reason for this behavior is that for these slender cracks the front surface effect tends

to increase K_I faster than the shape effect tends to decrease it in the range from $\phi = 0^o$ to approximately $\phi = 40^o$.

A cursory inspection of the curves of Figs. 18 through 21 reveals at least two general trends. It is apparent that for any given crack depth ratio a/t, the maximum K_I value is greater for slender cracks with small a/2c ratios than for the rounder cracks with larger a/2c ratios. Also, it is apparent that for any given a/2c ratio, the larger K_I values occur for the deeper cracks, or those with higher values of a/t.

The computations which were performed to obtain the results plotted in Figs. 18 through 21 used rectangular grids on the front and back surfaces similar to the one shown in Fig. 17. It was found that convergence difficulties existed for cases in which the plate thickness was approximately the same as the dimensions of the smallest rectangle. It was therefore necessary to revise the grid so that there were approximately twice as many rectangles near the origin of the grid. The revised grid has 79 rectangles, while the one shown in Fig. 17 has 55 rectangles. The grid with 79 rectangles was used whenever the crack depth "a" approached the size of the smallest rectangle. Grids of 62 and 32 rectangles were also used where the geometry of the problem being solved would permit the use of these configurations. The use of the proper grid insured that good convergence was attained, as evidenced by the fact that the contribution of the last cycle was generally less than one percent of the total stress intensity factor.

The stress intensity factor K_I, as shown in Figs. 18 through 21, smoothly approaches a definite value at $\phi = 90^o$. However, it is expected that there is a change in the nature of the crack tip singularity at the point where the tip of the crack intersects the surface of

the plate. This would mean that the curves do not represent the true behavior of the elastic solution there. Hartranft and Sih (28) have concluded that the mode one stress intensity factor tends to zero at the surface for a semicircular crack. They handled separately the singular and nonsingular portions of the stress on the surface of the plate. In addition, they used a very large number of rectangles and a large number of terms in the series expansions used to calculate the stresses. Smith (29) concluded that for the semicircular crack the level of approximation used here gives results within one or two percent over most of the crack border as compared with the results obtained from the more refined analysis of (28), although there can be a sizeable difference near the intersection of the crack tip with the front surface.

It is therefore reasonable to expect a similar behavior for this analysis which involves a semielliptical crack rather than a semicircular crack as considered in (29). The stress intensity factor K_1 at $\phi = 90^\circ$ has little practical importance, however, since the maximum occurs somewhere between the angle of $\phi = 0^\circ$ and 40°, as shown in Figs. 18 through 21 for semielliptical surface flaws.

Figure 22 presents the values of maximum K_1 from this analysis for a/2c values of 0.05, 0.1, 0.2, and 0.3. The curves for a/2c values of 0.4 and 0.5 were estimated by Shah and Kobayashi (17) from their solution for the elliptical crack near the surface of a half-space. The results for the two-dimensional edge crack (30) which represents the limiting solution are also shown in the figure. It has been argued that cracks having an a/2c ratio less than 0.1 closely approximate the behavior of a two-dimensional edge crack, but these results indicate

that even a crack having a length 20 times its depth is somewhat less severe than a two-dimensional edge crack.

2.0 Comparisons with Other Work

A comparison of the results of this study with those due to Shah and Kobayashi (17) is made in Fig. 23. Shah and Kobayashi obtained their results by assuming that the back surface effects are the same as the effect of the surface for an elliptical crack approaching the surface in a semi-infinite solid. They estimated the effect of the front surface, but chose to neglect the effect of the interaction between the front and back surfaces.

The surface interaction effect causes only slight changes in the results for values of a/2c = 0.3 and greater. Though not shown for a/2c = 0.3, the results of this study compare well with those of Shah and Kobayashi for a/2c = 0.3, and they approach closely for a/2c = 0.2. However, the curves from this study become relatively higher as a/2c is decreased to 0.1 and 0.05, indicating the growing importance of the interaction between the front and back surfaces for slender cracks.

The results of Fig. 22 were used to compute the fracture toughness values for a number of epoxy plates on which experiments were conducted by Smith (29). The fracture toughness K_{IC} was calculated as

$$K_{IC} = M_1 \sigma (\pi a/Q)^{\frac{1}{2}} . \qquad (7.1)$$

The nominal stress in the sample plate at the time of fracture is indicated by σ, and "a" is the depth of the crack. The flaw shape parameter Q is defined as $Q^{\frac{1}{2}} = E(k)$, the complete elliptic integral of the second kind. The term M_1 is the nondimensionalized form of K_1 and

is frequently called the magnification factor where the subscript indicates the mode one loading case.

Figure 24 presents a plot of fracture toughness values which were calculated from the experiments of (29) using the curves of Fig. 22. The data was used in equation (7.1) and was taken from a number of different epoxy plates having different average fracture toughness values. It was normalized by dividing the K_{IC} value for each sample by an average K_{IC} value for the epoxy plate from which the sample was taken. The average fracture toughness values which were used to normalize the data were calculated using only samples which had a/t values of 0.5 or less. As shown in the figure, the a/2c values ranged from about 0.13 to about 0.42. The normalized fracture toughness has a scatter band of approximately ±10 percent, and is relatively constant with variation in a/t, although it does drop slightly as a/t is increased. The constant trend of the normalized values indicates that the curves are valid and possess some practical utility for design and analysis situations in which linear fracture mechanics may be applied.

3.0 Advantages and Limitations of the Method

The alternating method, as used in this study, is capable of producing a reasonably accurate solution to the types of problems discussed here. The method is straightforward and requires no approximations from two dimensional theories to effect the desired solution.

Extremely good convergence can be realized but it is not always easily attained. As has been mentioned previously, convergence is quite dependent upon the number and size of the rectangles used in the grid. The desire for extreme accuracy would dictate the maximum number of rectangles possible. However, the total computer time used is a

function of the product of the number of front and back surface rectangles used, so a compromise is necessary.

The total computer time required for some typical configurations for the shear loading problem has been discussed in Chapter 5. The normal loading problem was usually run with a total of four cycles of iteration for each crack geometry. This number of cycles required 960 seconds of total computer time for 62 front and 32 rear rectangles, 1220 seconds for 55 rectangles on each surface, and 2000 seconds for 79 rectangles on each surface. The entire program was cataloged on permanent file within the computer, so none of the time mentioned above was lost to the CDC 6400 compiler.

Accuracy of the infinite solid solution is dependent upon the preciseness with which the method of least squares is able to match the calculated stresses with the proper polynomial expression. A polynomial with more terms than the number allowed in a third-degree polynomial would undoubtedly increase the accuracy of the curve fit, but more terms were impossible to tolerate for reasons already mentioned.

One of the limitations to the alternating method as it is presently used is its restriction to geometric configurations in which the front and back surfaces are parallel. The method is also limited to finite thickness bodies whose width is great enough so that no effects are realized from the presence of any side surfaces. This would pose a problem if solutions were desired for some geometries where the width effect could no longer be ignored.

Chapter 8

CONCLUSION

1.0 Discussion

A semielliptical surface crack located in the surface of a finite thickness solid and subjected to two different conditions of loading is considered. The first condition of loading is one in which shear stresses are applied to the surface of the crack parallel to the semimajor axis. The second loading case is the one in which normal loading is applied to the surface of the crack in a direction perpendicular to the plane of the crack. The alternating method was used in each of the two loading cases to solve the problem.

As a necessary part of the analysis, a solution was presented which developed the mode two and mode three stress intensity factors for an embedded elliptical crack subjected to nonuniform shear stresses. Additional equations were derived for the residual stress components on the crack surface which resulted from the freeing of the surfaces of the plate of stresses during the alternating technique.

Results were computed and presented graphically for the problem in which a uniform shear stress was applied to the surface of the crack and parallel to the semimajor axis of the ellipse, while no initial loading was applied in the direction parallel to the semiminor axis. Crack shapes were varied from a/2c ratios of 0.05 to 0.40 whereas crack depth ratios a/t were varied from 0.2 to 0.9. When compared to the maximum K_2 and K_3 values for embedded ellipses, the results revealed that there was only a slight change in the maximum K_2 and K_3 values for similar semielliptical cracks having low a/t ratios.

Both K_2 and K_3 became substantially larger as the crack depth a/t was increased, although K_3 experienced a significantly greater increase than did K_2. The maximum value of the mode three stress intensity K_3 for a crack with a/2c of 0.2 increased by 15.1 and 31.2 percent as a/t was increased to 0.8 and 0.9, respectively. The maximum mode two stress intensity factor K_2 for the corresponding geometries increased by 6.0 and 7.1 percent, respectively. Similar increases occur for other problem geometries, so these factors can play an important role in situations where mixed mode loading can occur.

The normal loading problem was solved in a manner which was essentially identical to the one used for the shear problem. The alternating method was again used to obtain the stress intensity factors, although it was the mode one factor K_1 which was of interest in this case.

Computer calculations were made and results were plotted for the case in which a uniform normal stress was applied to the surface of the crack in a direction which was perpendicular to the plane of the crack. Emphasis was placed on slender cracks, so runs were made for cases in which the crack shapes a/2c varied from 0.05 to 0.3 as crack depth ratios a/t were varied from 0.2 to 0.95.

The maximum value for the mode one stress intensity factor K_1 increases for any particular crack depth a/t as the crack becomes more slender with a decreasing a/2c ratio. Likewise, K_1 increased very significantly as the a/t ratio was increased for any particular a/2c value. Very slender cracks of low a/2c ratios and high a/t ratios produce high mode one stress intensity factors, and so are of special importance to the designer. Additionally, the maximum stress intensity

does not always occur at the deepest part of the crack, but can occur up to 40 or 50 degrees from that point.

Results from this study were compared with those obtained by other researchers who neglected the effects of the interaction between the front and back surfaces. The results compare well for cracks having a/2c of 0.2 and greater, but some difference in the results of the two studies is apparent for lower a/2c ratios, indicating the importance of this effect.

The results of this study were used to calculate the fracture toughness values for a large number of epoxy plates on which mode one tests were made. When normalized, these fracture toughness values are nearly constant, thus indicating the validity of the calculated results.

2.0 Recommendations

The complex loading of today's structures makes either of the two loadings discussed incomplete or inadequate when considered alone. When more than one mode is acting along the crack border, failure of the part becomes a function of all nonzero stress intensity factors. Very little work has been done on developing a theoretically or experimentally obtained mixed mode fracture criterion. This criterion is an urgent requirement if information such as that obtained in this study is to be employed usefully in the field of applied fracture mechanics.

As presently developed, the alternating method is limited to geometric configurations in which the front and back surfaces are parallel. This restriction on the relative placement of the surfaces does not allow the solution to be obtained for a large class of problems. A new technique utilizing a better method of obtaining the solution to stresses in an uncracked body of general shape with general

boundary conditions, such as a three-dimensional finite element method, would greatly increase the problem solving capabilities of this method if it could be done without extensive increases in computer time requirements.

REFERENCES

1. Kobayashi, A.S., "Fracture Mechanics," in Experimental Techniques in Fracture Mechanics. Edited by A.S. Kobayashi. Westport, Connecticut: Society for Experimental Stress Analysis, SESA Monograph No. 1, 1973.

2. Inglis, C.E , "Stresses in a Plate Due to the Presence of Cracks and Sharp Corners," Transactions of the Institute of Naval Architects, Vol. 55, 1913.

3. Griffith, A.A., "The Phenomena of Rupture and Flow in Solids," Philosophical Transactions of the Royal Society (London), Series A, Vol. 221, 1920.

4. Sneddon, I.N., "The Distribution of Stress in the Neighborhood of a Crack in an Elastic Solid," Proceedings of the Royal Society (London), Series A, Vol. 187, 1946.

5. Green, A.E. and I.N. Sneddon, "The Distribution of Stress in the Neighborhood of a Flat Elliptical Crack in an Elastic Solid," Proceedings of the Cambridge Philosophical Society, Vol. 46, 1950.

6. Shah, R.C. and A.S. Kobayashi, "Stress Intensity Factor for an Elliptical Crack Under Arbitrary Normal Loading," Journal of Engineering Fracture Mechanics," Vol. 3, No. 1, July 1971.

7. Irwin, G.R., "Crack Extension Force for a Part-Through Crack in a Plate," Journal of Applied Mechanics, Vol. 33, No. 4, December 1966.

8. Smith, F.W., "Stresses Near a Semi-Circular Edge Crack," Ph.D. Thesis, University of Washington, 1966.

9. Smith, F.W., A.F. Emery and A.S. Kobayashi, "Stress Intensity Factors for Semicircular Cracks," Journal of Applied Mechanics, Vol. 34, December 1967.

10. Lachenbruch, A.H., "Depth and Spacings of Tension Cracks," Journal of Geophysical Research, Vol. 66, No. 12, 1961.

11. Alavi, M.J., "Stresses Near a Circular Crack in a Half-Space," Ph.D. Thesis, Colorado State University, 1968.

12. Smith, F.W. and M.J. Alavi,"Stress Intensity Factors for a Penny-Shaped Crack in a Half-Space," Journal of Engineering Fracture Mechanics, Vol. 3, No. 2, 1971.

13. Smith, F.W. and M.J. Alvai, "Stress Intensity Factors for a Part-Circular Surface Flaw," Proceedings of the First International Conference on Pressure Vessel Technology, Delft, Holland, 1969.

14. Thresher, R.W., "A Surface Crack in a Finite Solid," Ph.D. Thesis, Colorado State University, 1970.

15. Thresher, R.W. and F.W. Smith, "Stress Intensity Factors for a Surface Crack in a Finite Solid," Journal of Applied Mechanics, Vol. 39, No. 1, March 1972.

16. Shah, R.C. and A.S. Kobayashi, "Stress Intensity Factors for an Elliptical Crack Approaching the Surface of a Semi-Infinite Solid," Boeing Aerospace Company Document, No. D-180-14494-1, 1971.

17. Shah, R.C. and A.S. Kobayashi, "Stress Intensity Factors for an Elliptical Crack Approaching the Surface of a Semi-Infinite Solid," International Journal of Fracture, Vol. 9, No. 2, June 1973.

18. Shah, R.C. and A.S. Kobayashi, "Stress Intensity Factor for an Elliptical Crack Approaching the Surface of a Plate in Bending," in Stress Analysis and Growth of Cracks. Philadelphia: American Society for Testing and Materials, ASTM STP 513, 1972.

19. Segedin, C.M., "A Penny-Shaped Crack Under Shear," Proceedings of the Cambridge Philosophical Society, Vol. 47, 1950.

20. Westman, R.A., " Asymmetric Mixed Boundary-Value Problem of the Elastic Half-Space," Journal of Applied Mechanics, Vol 32, No. 2, June 1965.

21. Eshelby, J.D., "The Determination of the Elastic Field of an Ellipsoidal Inclusion and Related Problems," Proceedings of the Royal Society, Series A, Vol. 241, 1957.

22. Kassir, M.K. and G.C. Sih, "Three-Dimensional Stress Distribution Around an Elliptical Crack Under Arbitrary Loadings," Journal of Applied Mechanics, Vol. 33, No. 3, September 1966

23. Love, A.E.H., A Treatise on the Mathematical Theory of Elasticity. New York: Dover Publications, 1944.

24. Love, A.E.H., "On Stress Produced in a Semi-Infinite Solid by Pressure on Part of the Boundary," Philosophical Transactions of the Royal Society, Series A, Vol. 228, 1929.

25. Segedin, C.M., "Some Three-Dimensional Mixed Boundary Value Problems in Elasticity," Report, Department of Aeronautics and Astronautics, University of Washington, Seattle, Washington, June 1967.

26. Byrd, P.F. and M.D. Friedman, Handbook of Elliptic Integrals. Berlin: Springer-Verlag, 1971.

27. Abramawitz, M. and I.A. Stegum, Handbook of Mathematical Functions. New York: Dover Publications, Inc., 1965.

28. Hartranft, R.J. and G.C. Sih, "Alternating Method Applied to Edge and Surface Crack Problems," in Mechanics of Fracture 1--Methods of Analysis and Solutions of Crack Problems. Edited by G.C. Sih. Leyden, The Netherlands: Noordhoff International Publishing, 1973.

29. Smith, F.W., "The Elastic Analysis of the Part-Circular Surface Flaw Problem by the Alternating Method," in The Surface Crack: Physical Problems and Computational Solutions. Edited by J.L. Swedlow. New York: American Society of Mechanical Engineers, 1972.

30. Brown, W.F. and J.E. Srawley, Plane Strain Crack Toughness Testing of High Strength Metallic Materials. Philadelphia: American Society for Testing and Materials, ASTM STP 410, 1966.

FIGURES

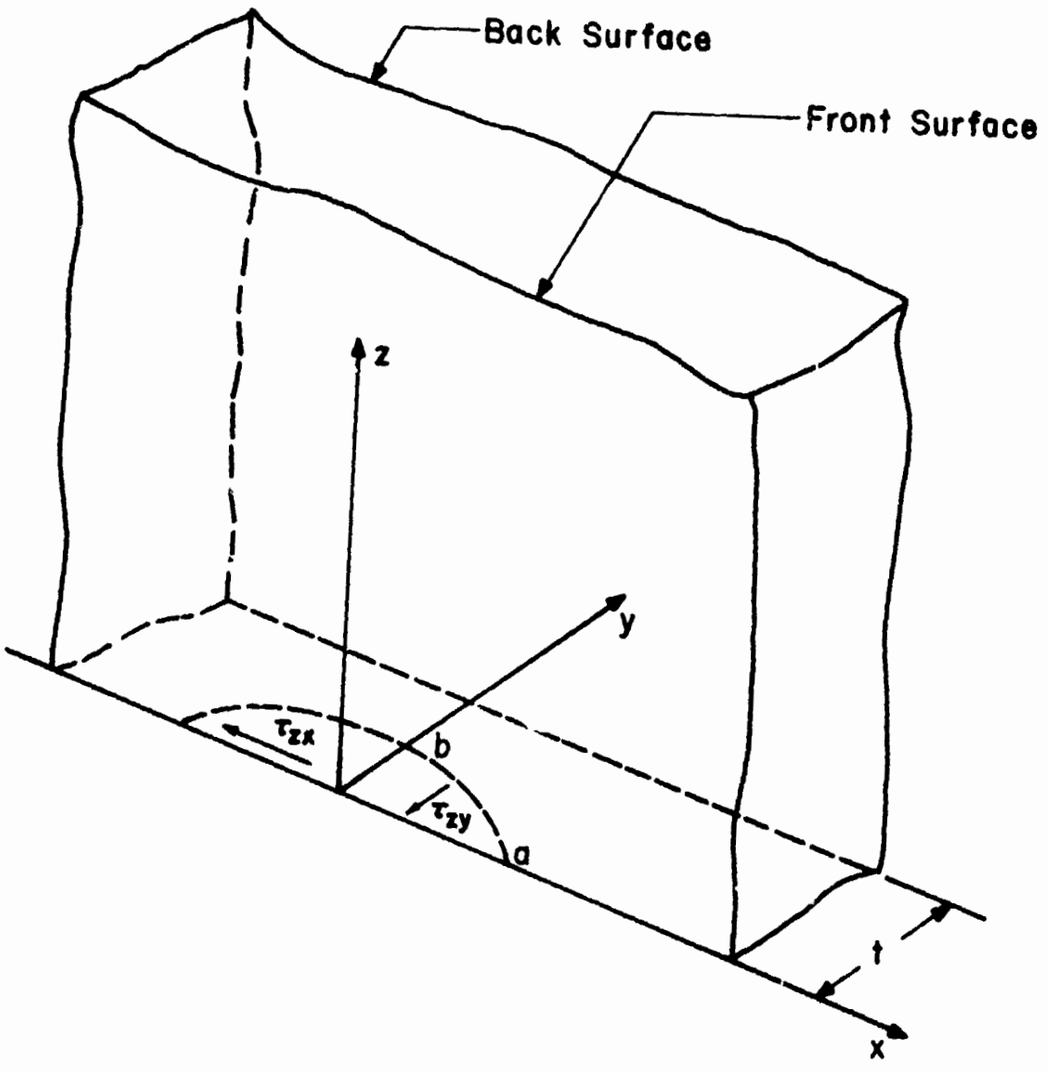

Figure 1. Semielliptical Surface Flaw in a Finite Thickness Plate

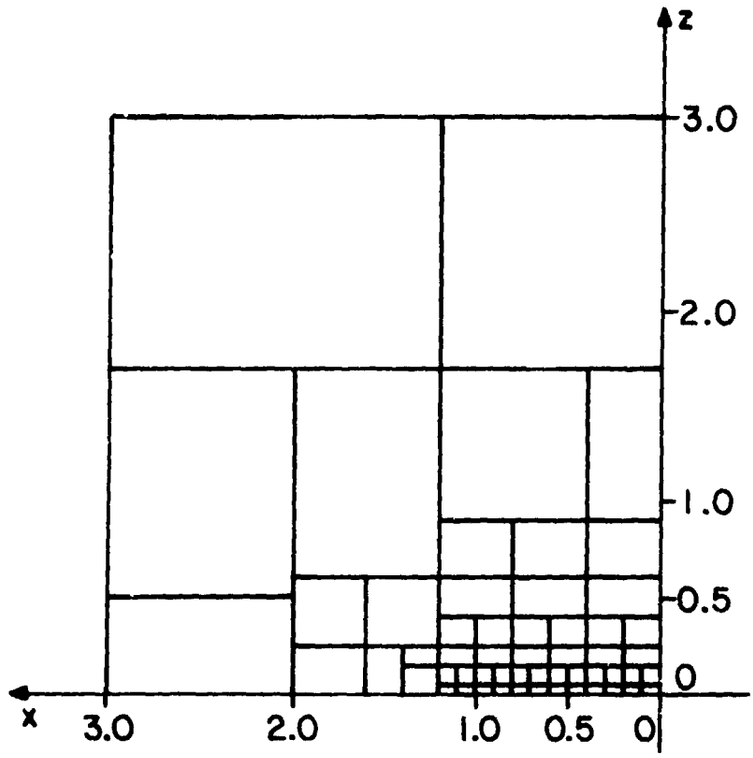

Figure 2. Arrangement of Surface Rectangles for the Shear Problem

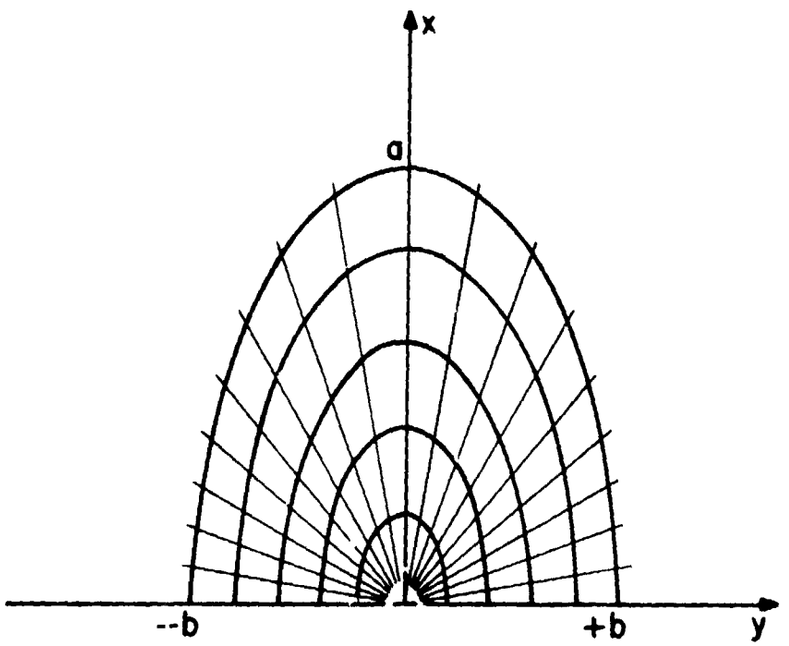

Figure 3. Location of Points on the Crack Surface

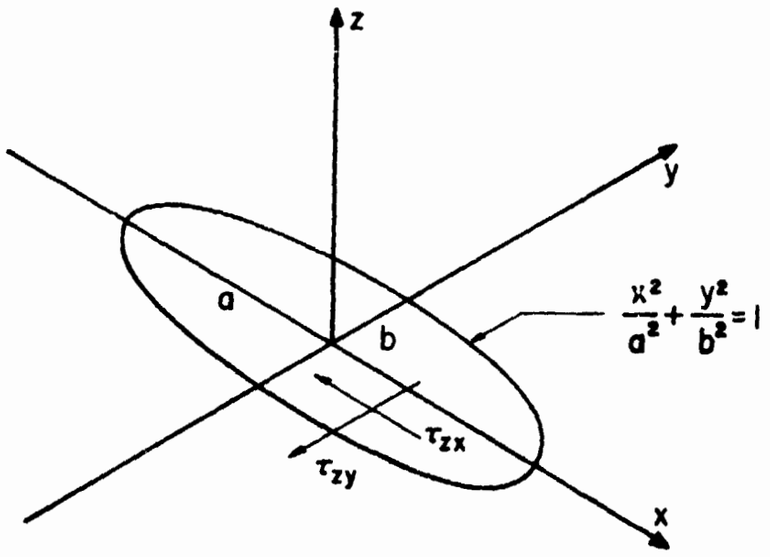

Figure 4. Flat Elliptical Crack Subjected to Nonuniform Shear

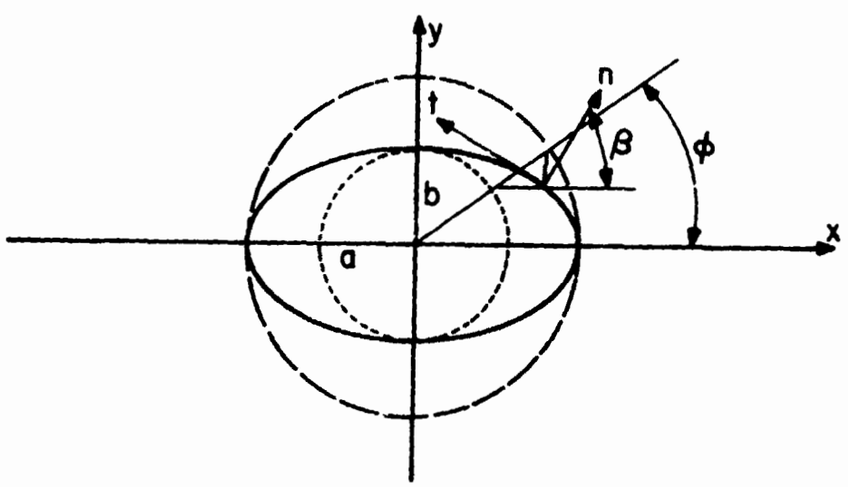

Figure 5. Parametric Angle ϕ, Normal and Tangential Directions n and t and the Angle β for an Elliptical Crack

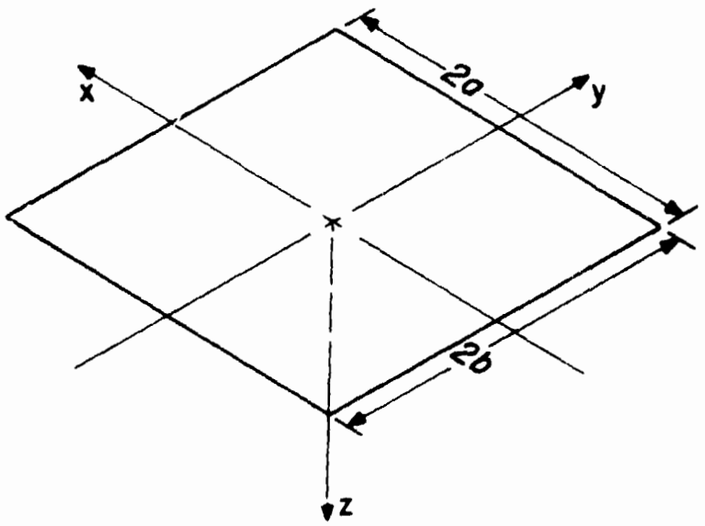

Figure 6. Local Coordinate System for a Typical Surface Rectangle

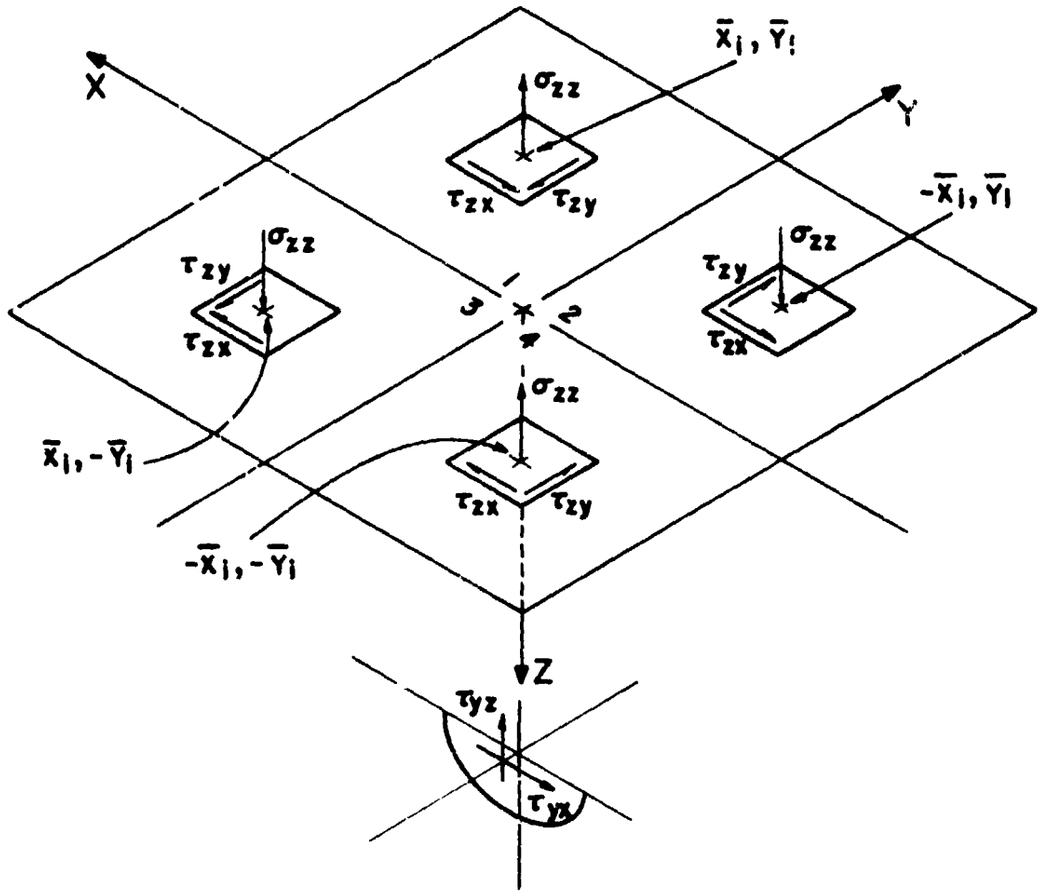

Figure 7. Coordinate System for the Half-Space Solution

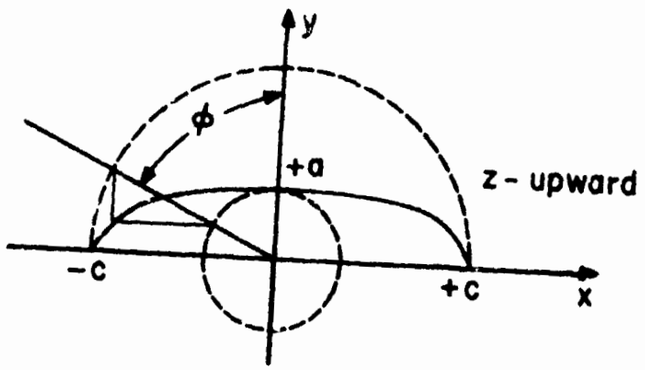

Figure 8. Coordinate System for the Elliptical Crack

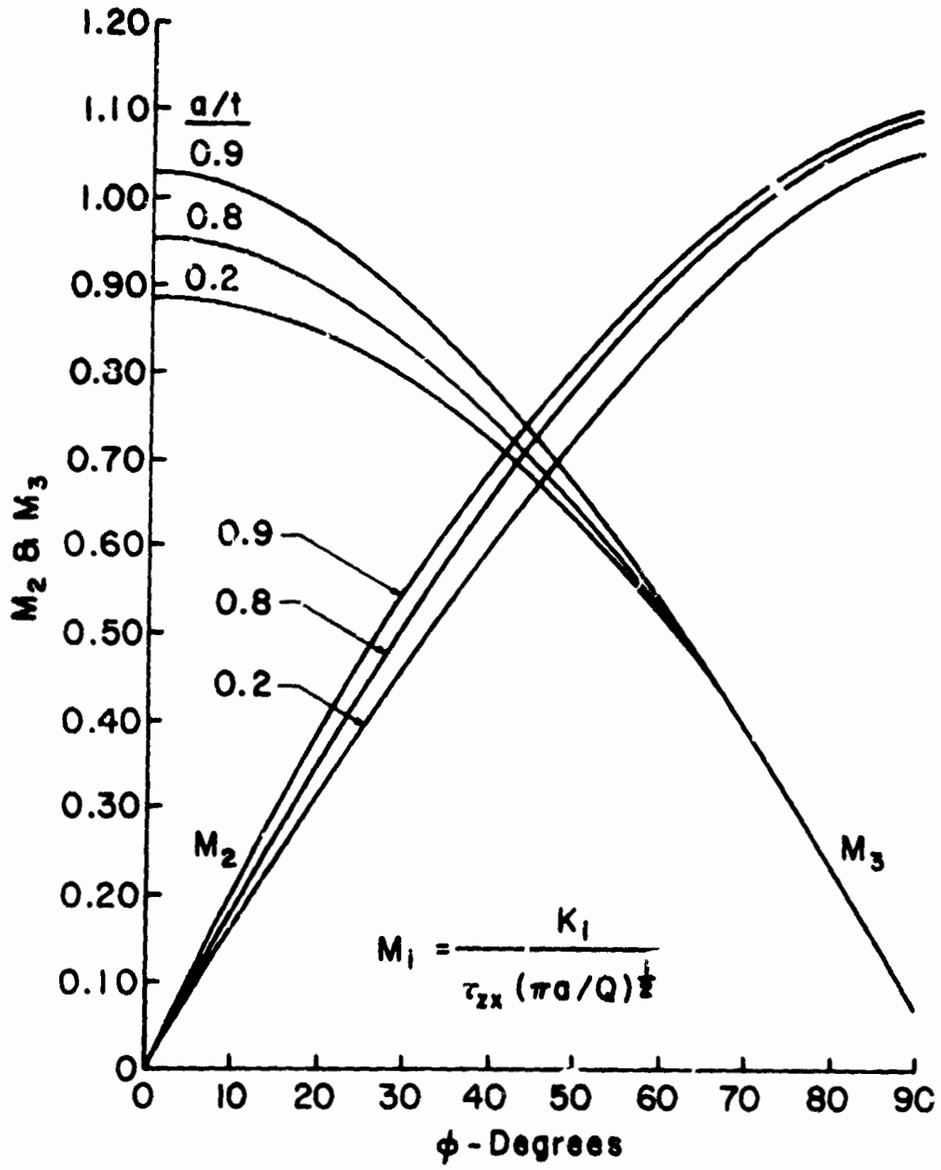

Figure 9. Stress Intensity Factors for a Surface Crack with Uniform Shear Applied Parallel to the Major Axis; a/2c = 0.40

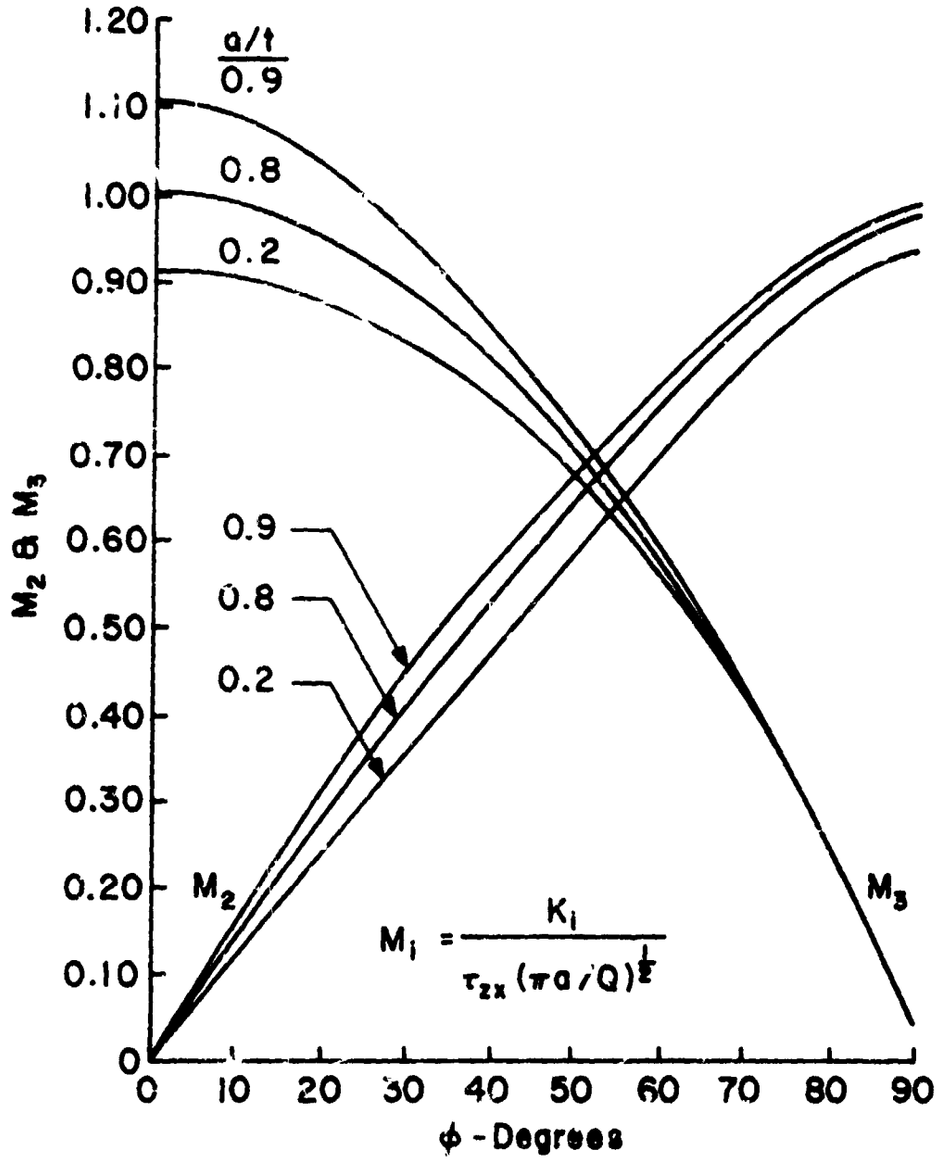

Figure 10. Stress Intensity Factors for a Surface Crack with Uniform Shear Applied Parallel to the Major Axis; a/2c = 0.30

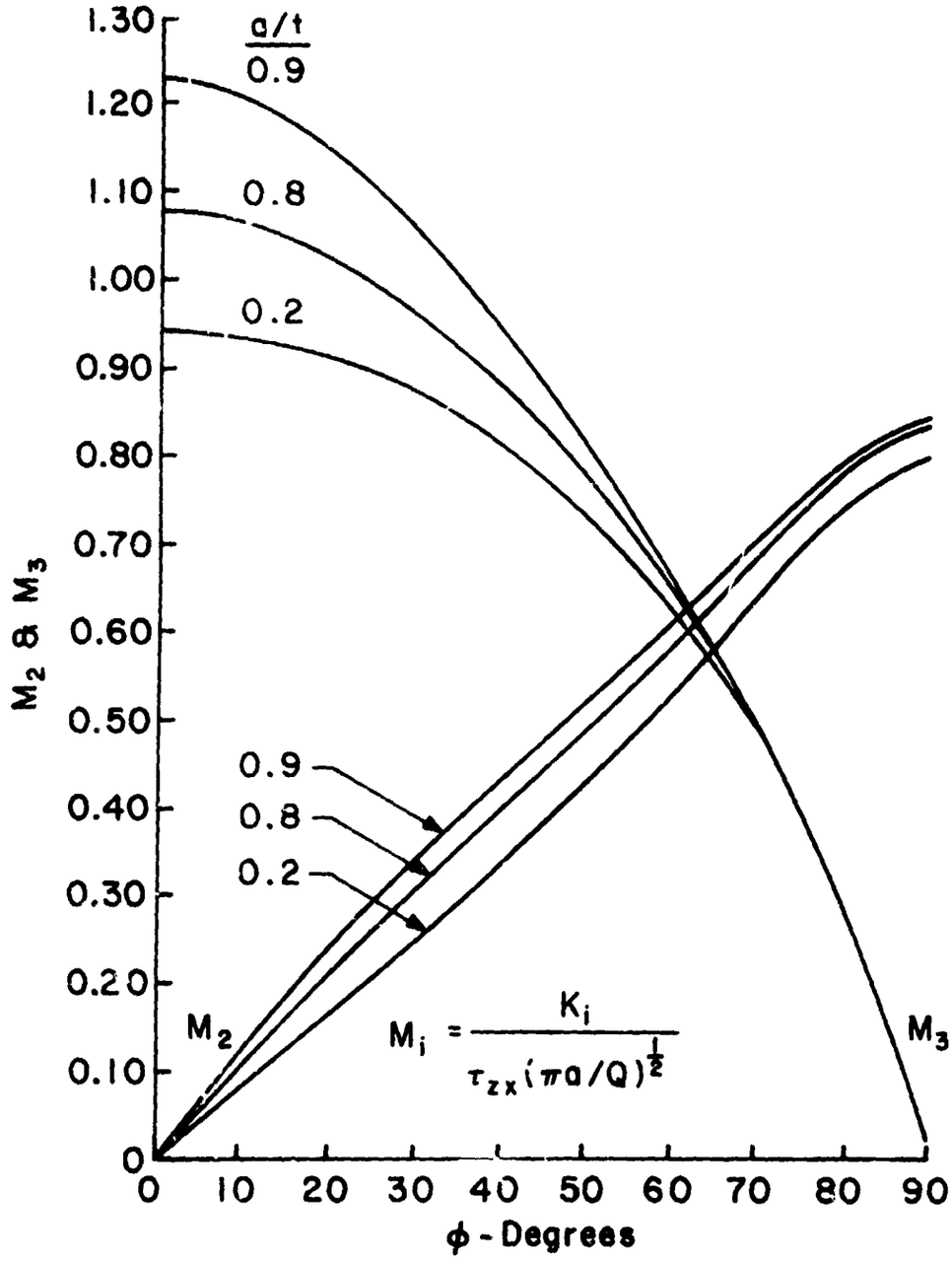

Figure 11. Stress Intensity Factors for a Surface Crack with Uniform Shear Applied Parallel to the Major Axis; a/2c = 0.20

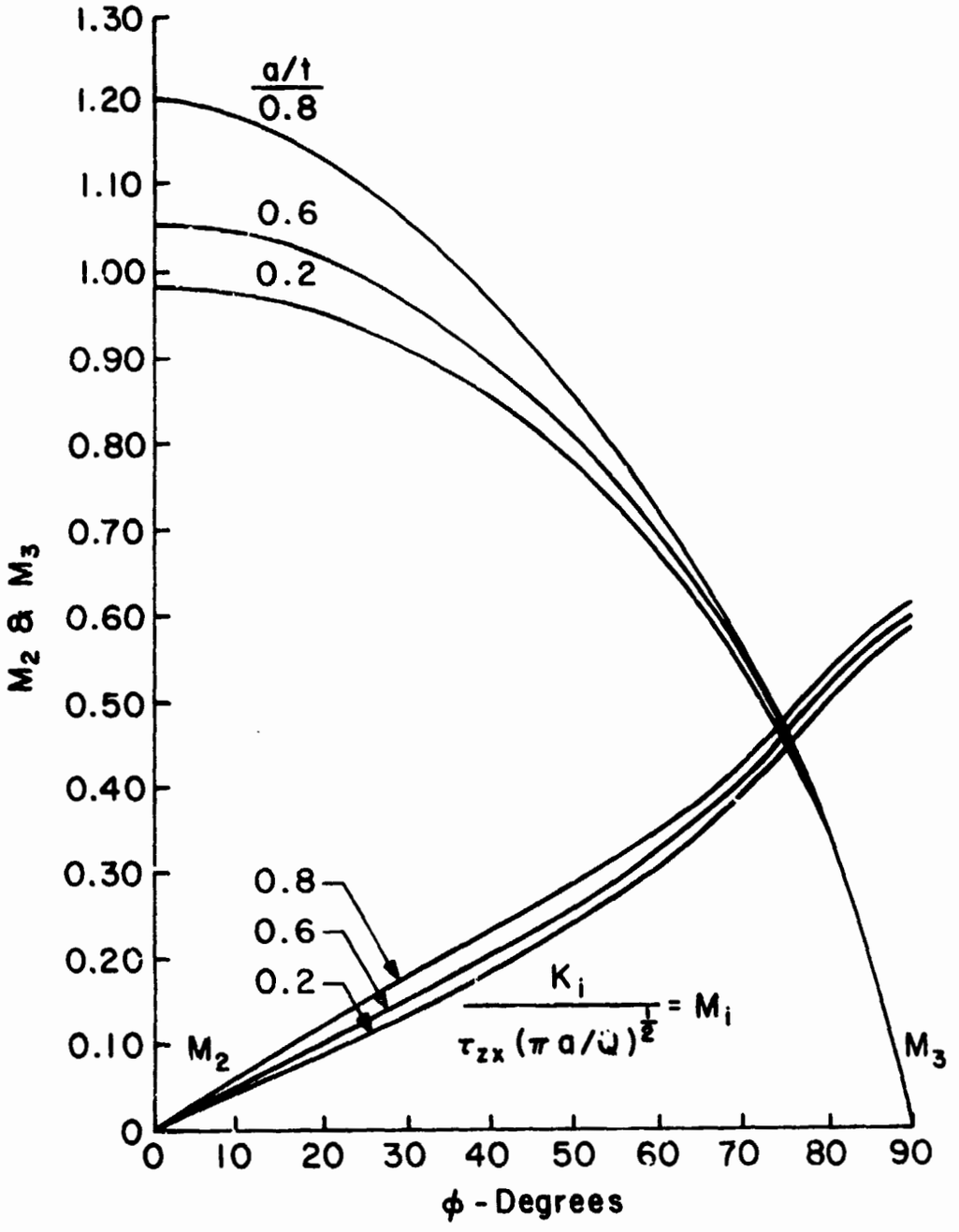

Figure 12. Stress Intensity Factors for a Surface Crack with Uniform Shear Applied Parallel to the Major Axis; a/2c = 0.10

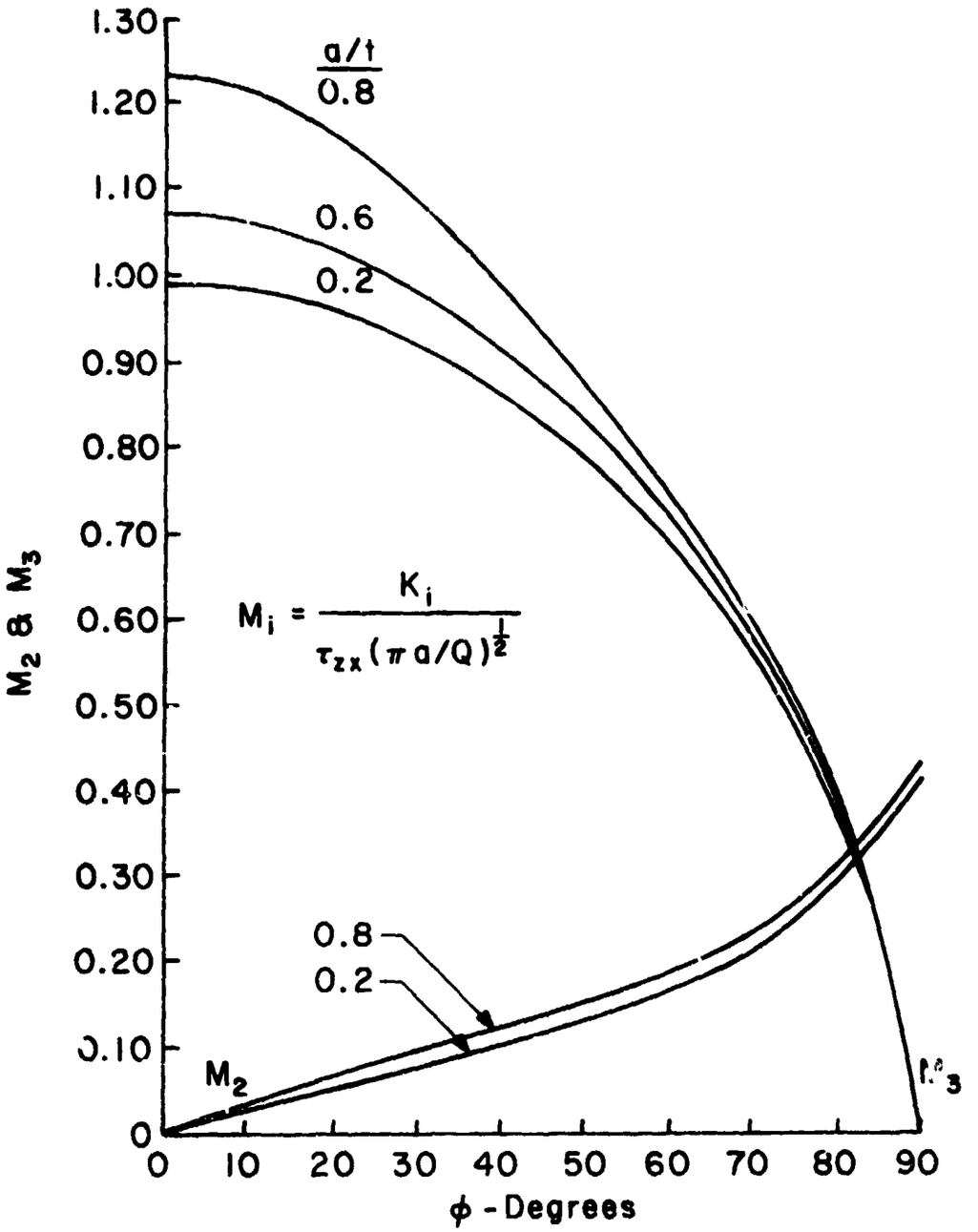

Figure 13. Stress Intensity Factors for a Surface Crack with Uniform Shear Applied Parallel to the Major Axis; a/2c = 0.05

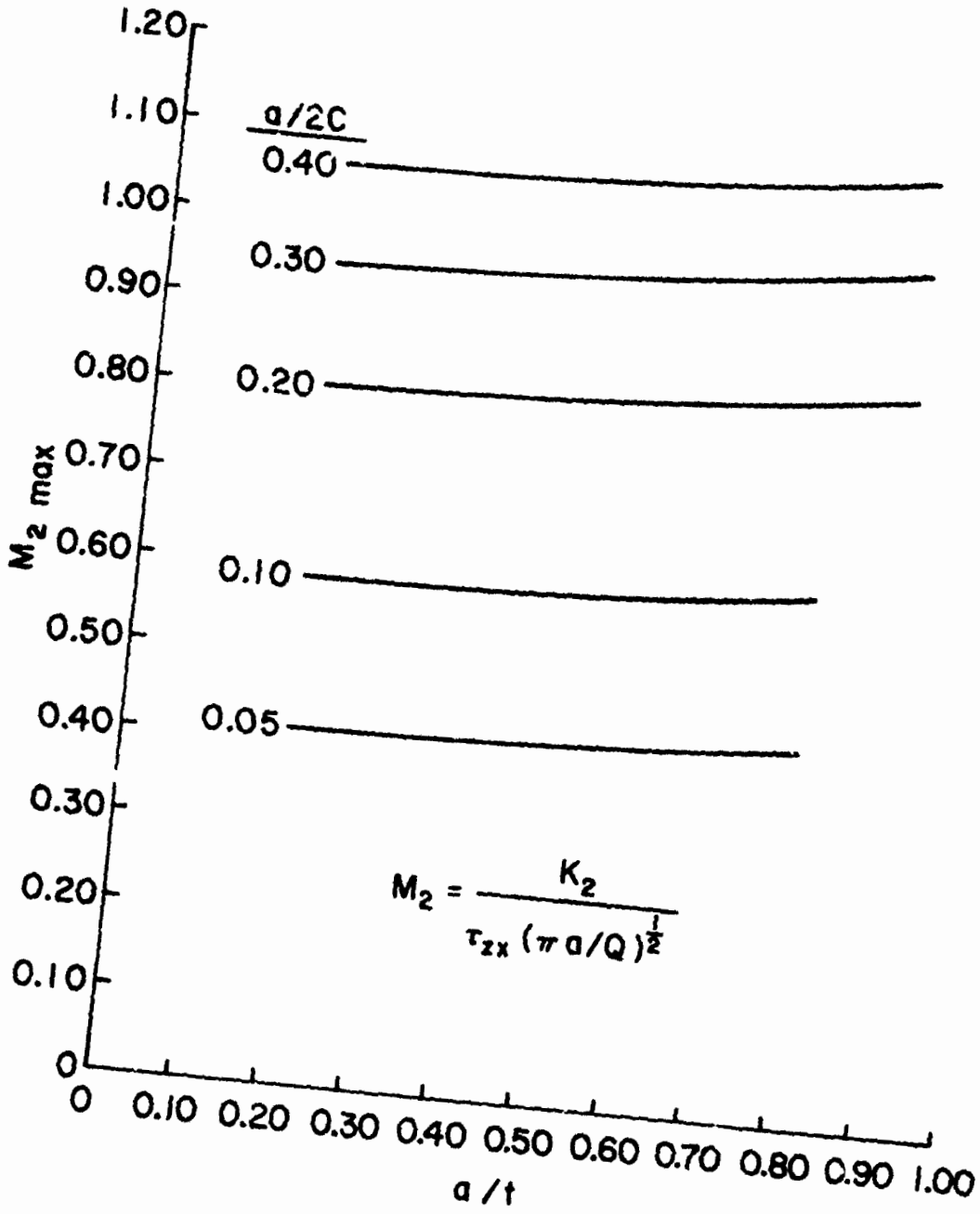

Figure 14. Maximum Mode Two Stress Intensity Factor for a Semielliptical Surface Crack

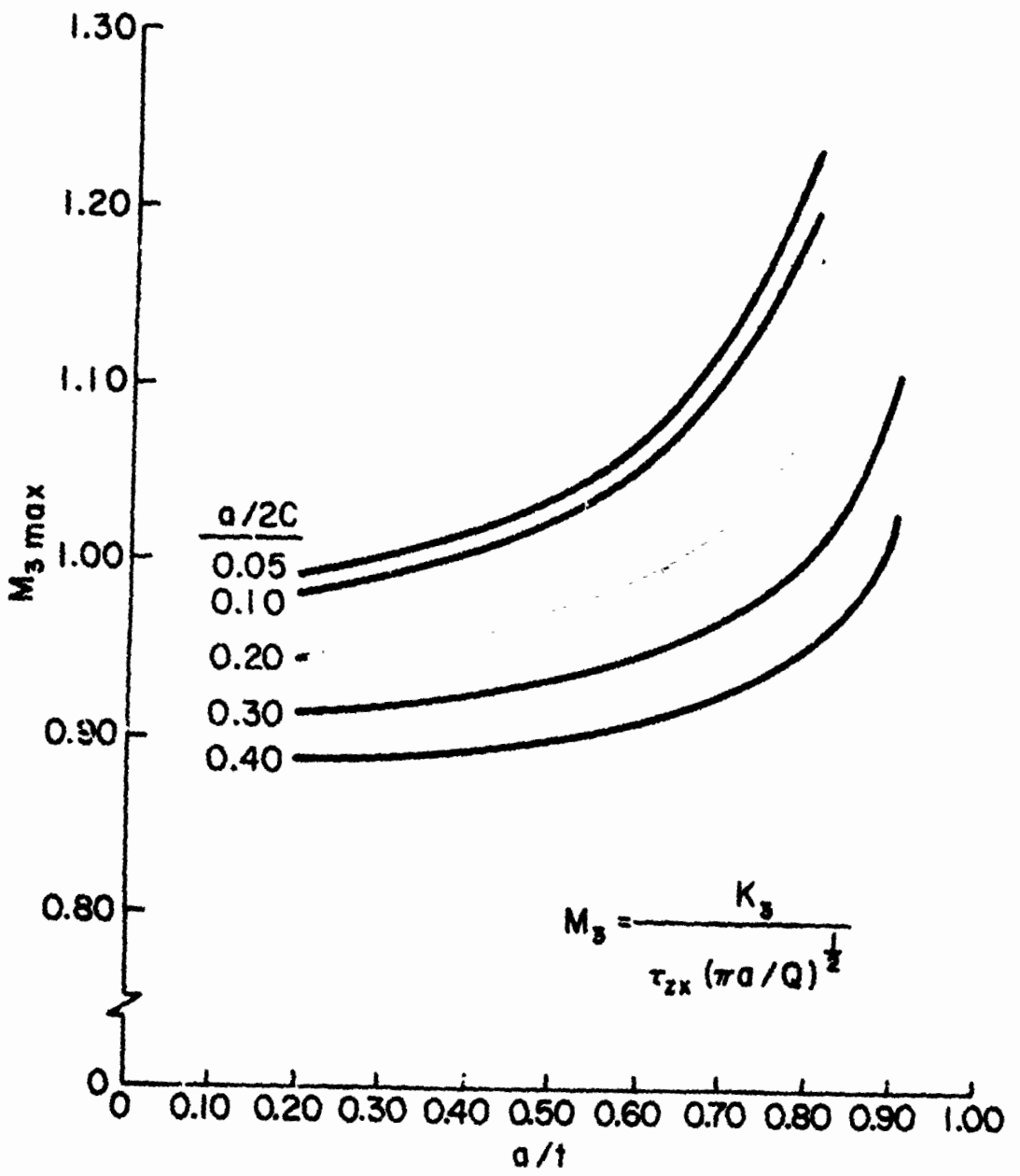

Figure 13. Maximum Mode Three Stress Intensity Factor for a Semielliptical Surface Crack

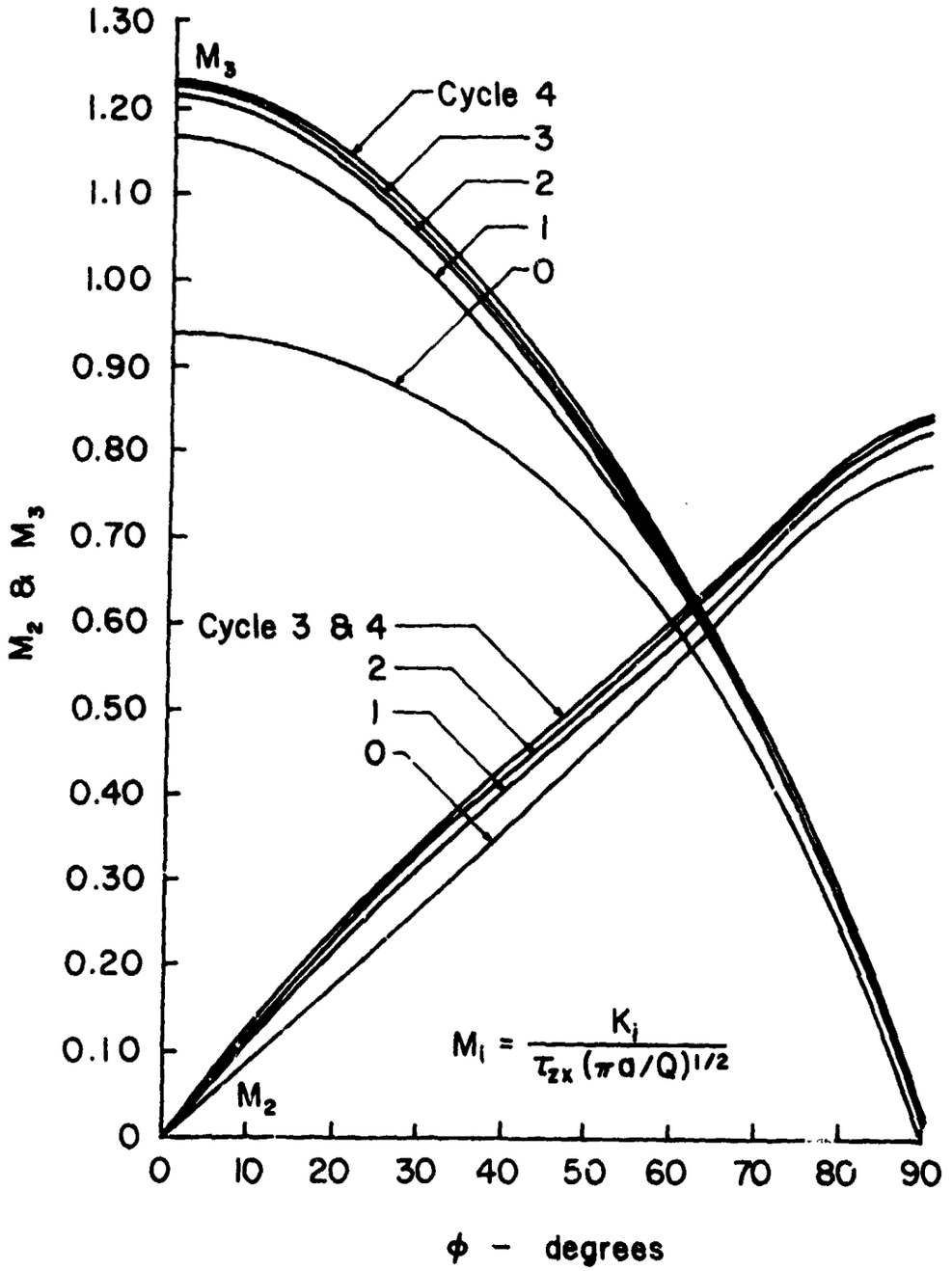

Figure 16. Stress Intensity Factors for Successive Cycles of Iteration; a/2c = 0.20 and a/t = 0.90

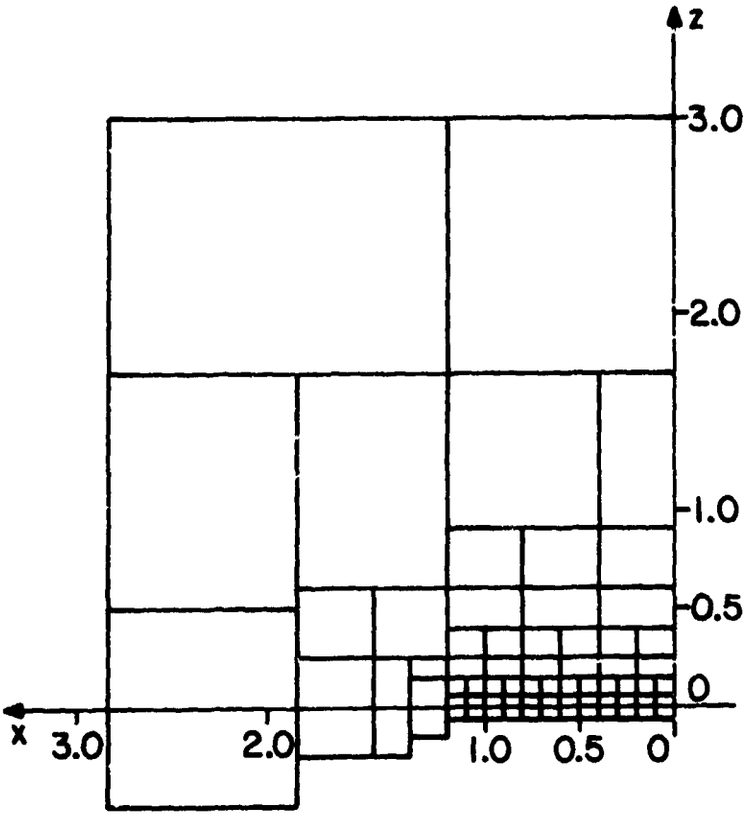

Figure 17. Arrangement of Surface Rectangles for the Normal Loading Problem

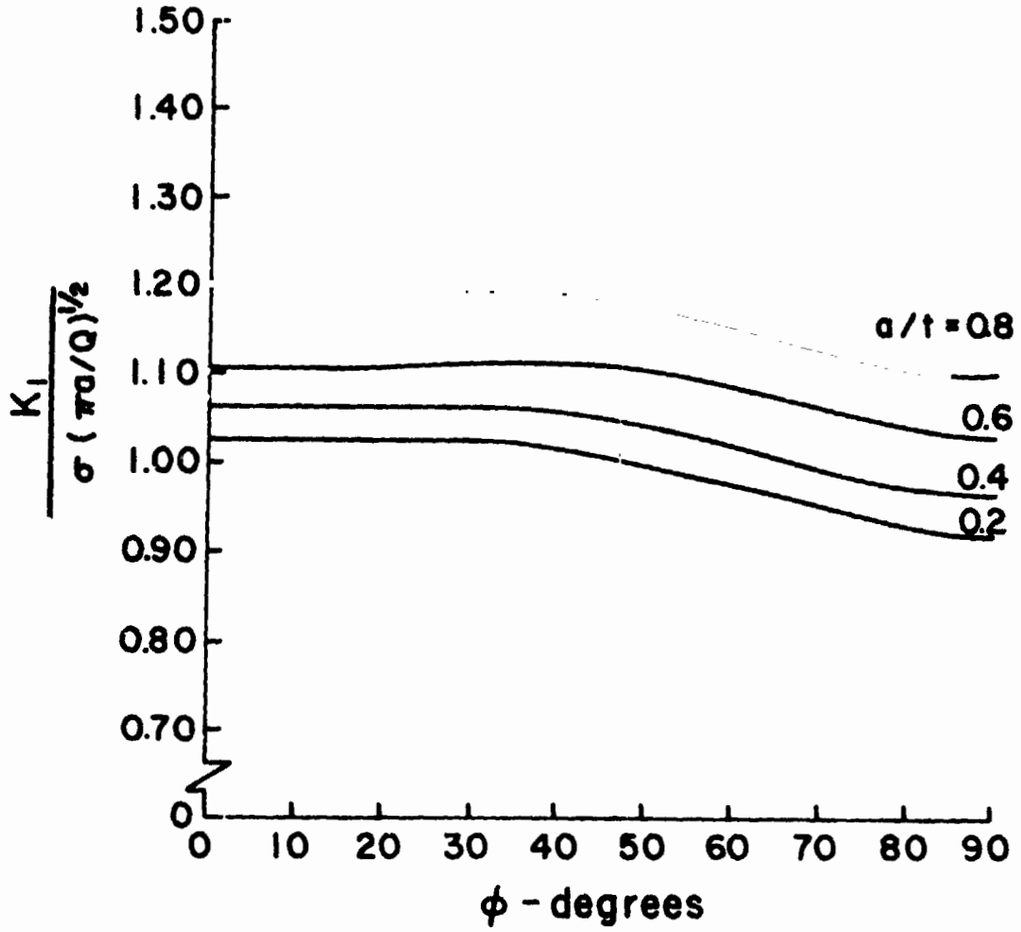

Figure 18. Stress Intensity Factor for a Surface Crack Subjected to Normal Loading; a/2c = 0.30

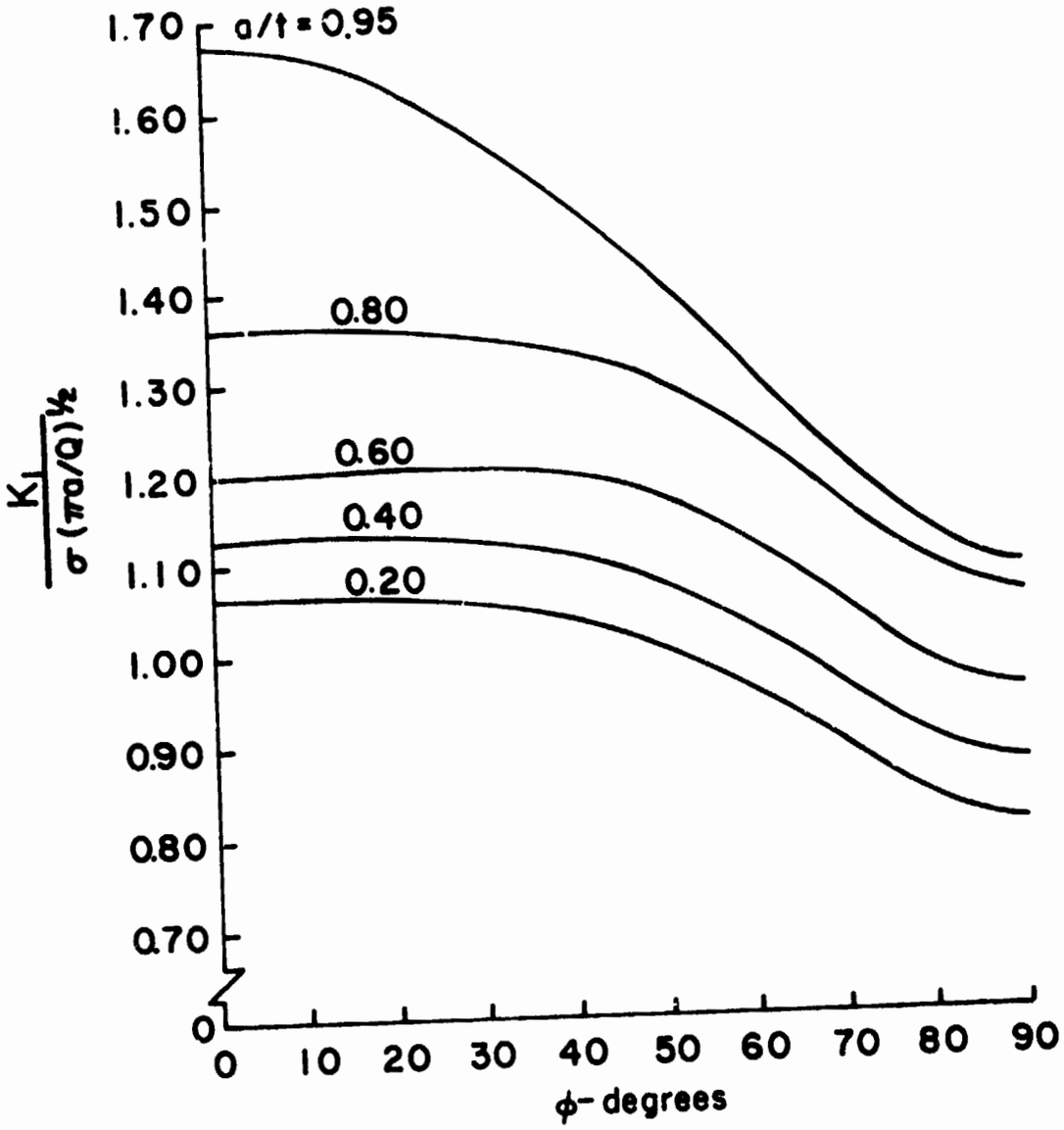

Figure 19. Stress Intensity Factor for a Surface Crack Subjected to Normal Loading; a/2c = 0.20

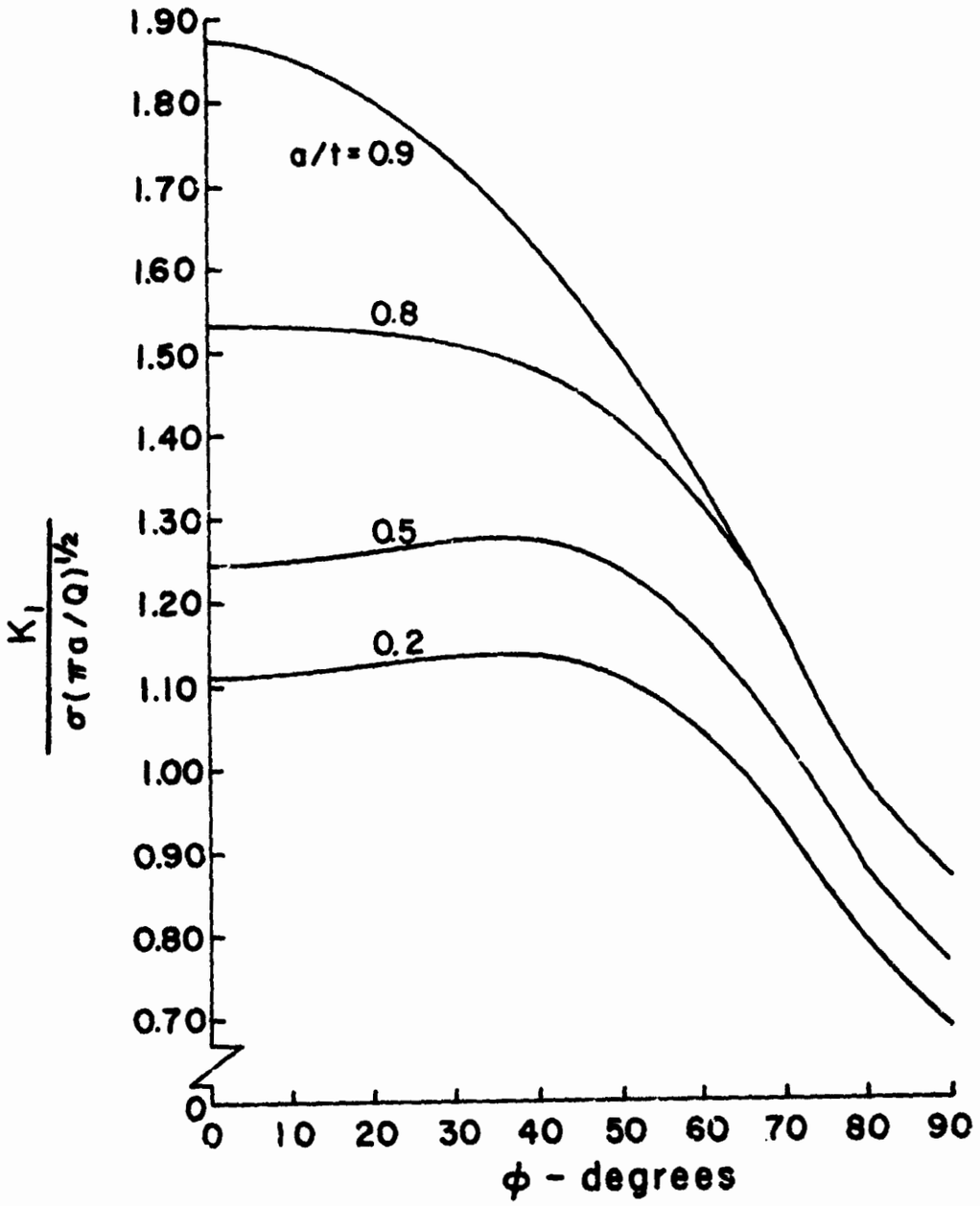

Figure 20. Stress Intensity Factor for a Surface Crack Subjected to Normal Loading; a/2c = 0.10

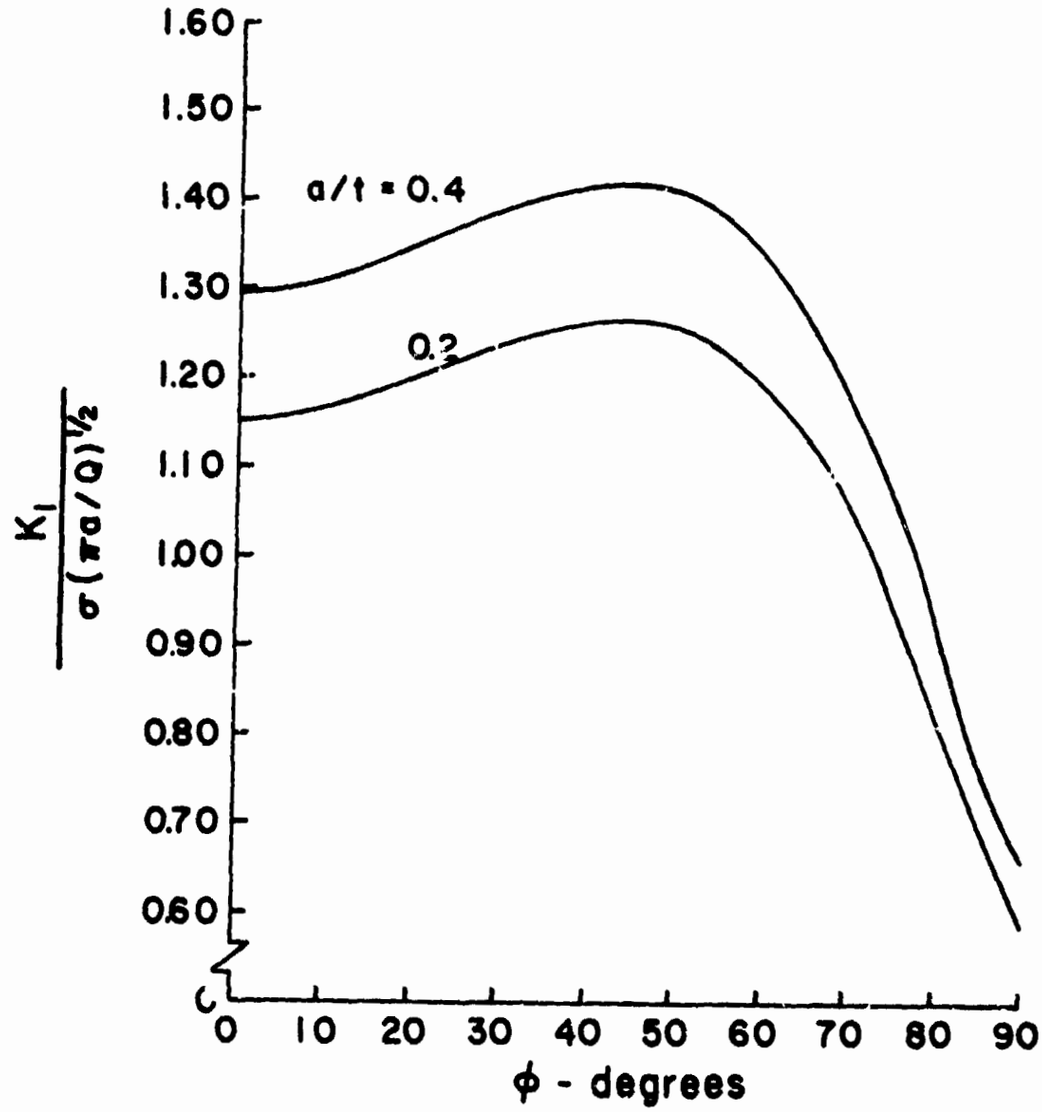

Figure 21. Stress Intensity Factor for a Surface Crack Subjected to Normal Loading; a/2c = 0.05

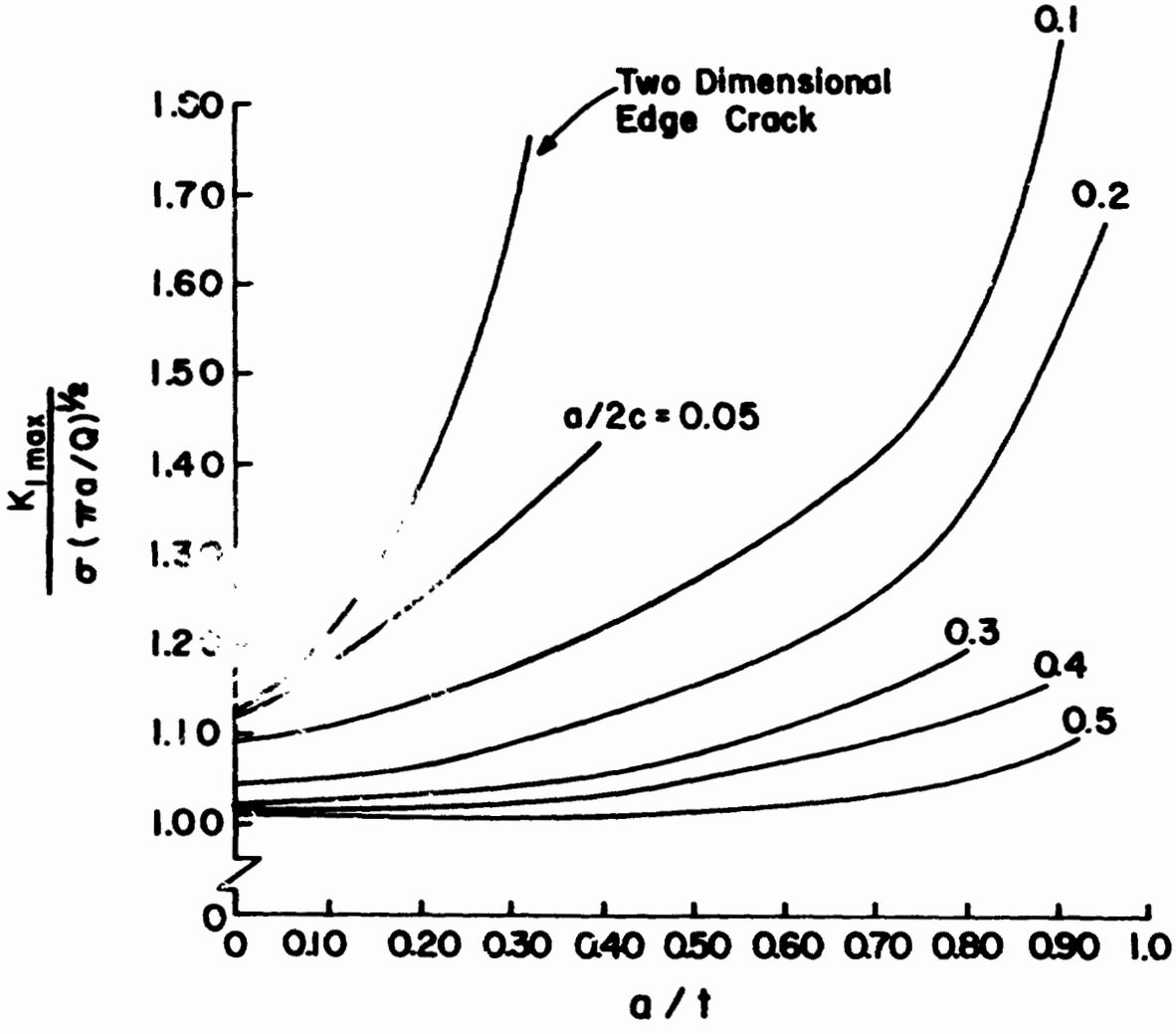

Figure 22. Maximum Mode One Stress Intensity Factor for a Semielliptical Surface Crack

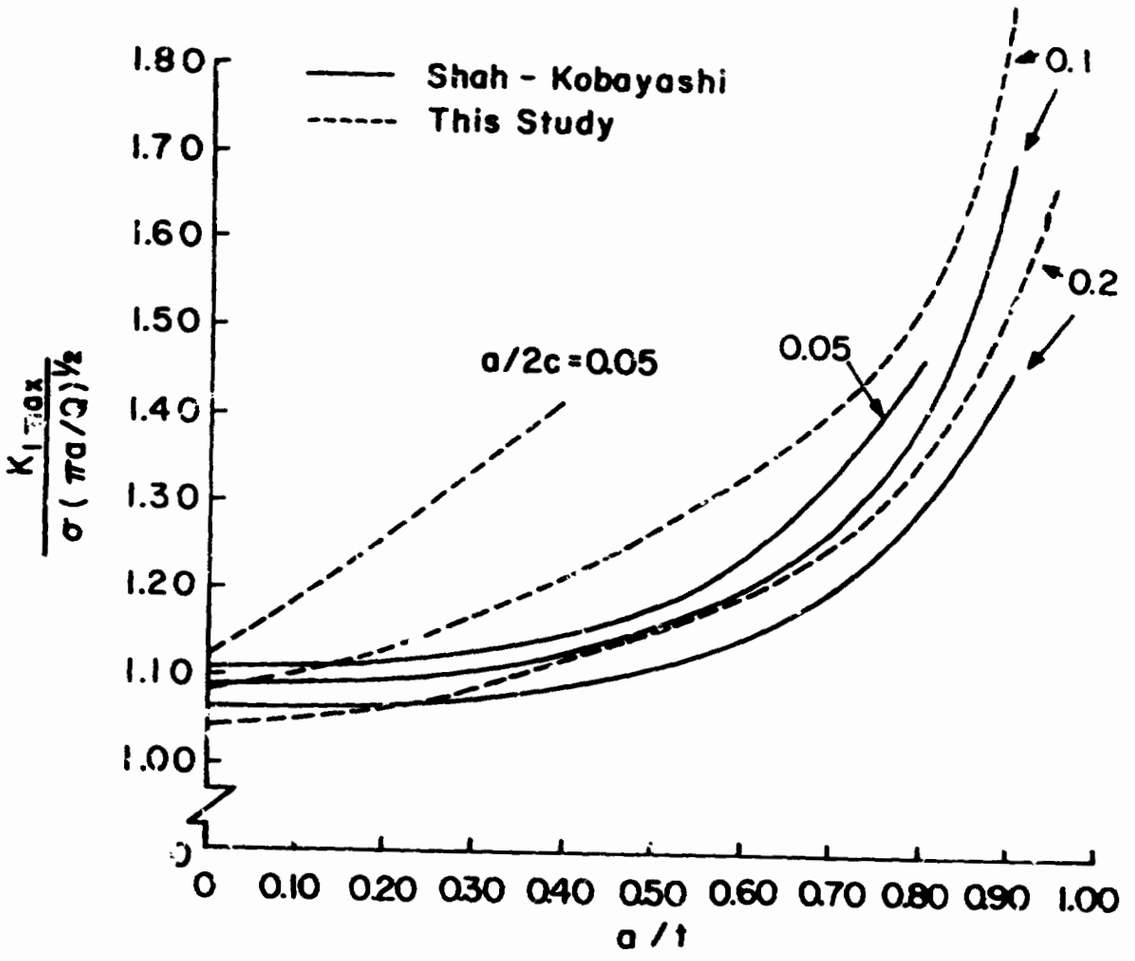

Figure 25. Comparison of Theoretical Mode One Stress Intensity Factors for a Semielliptical Surface Crack

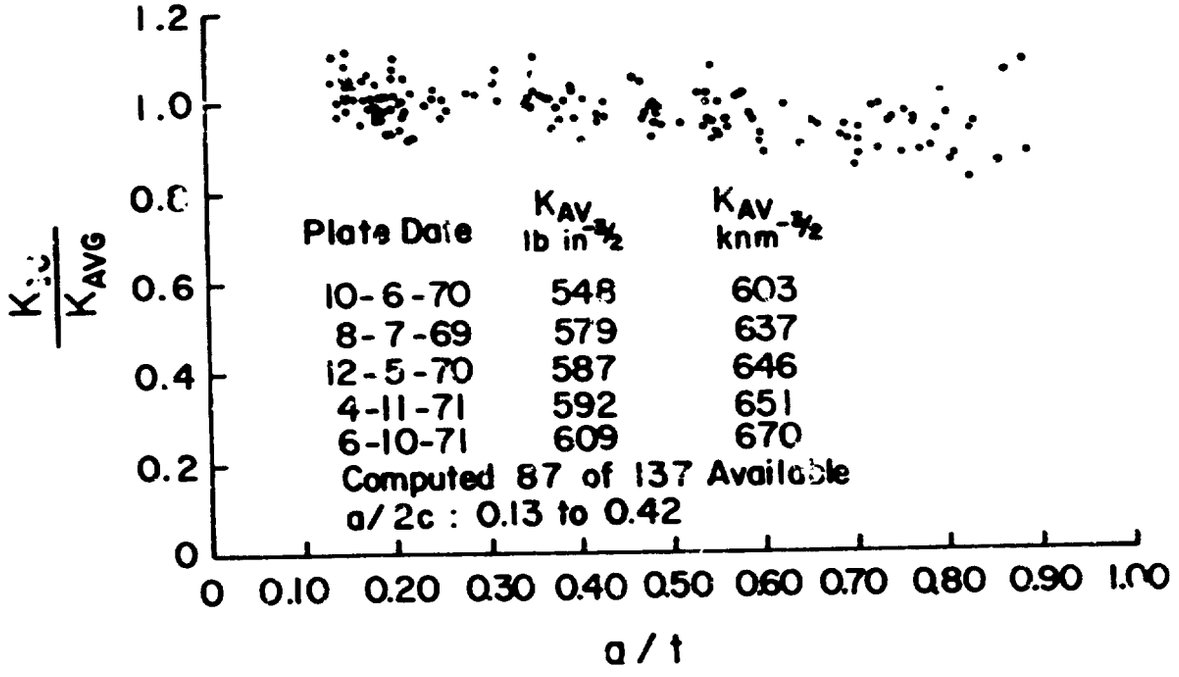

Figure 24. Fracture Toughness Data for Epoxy

APPENDIXES

C - 2

APPENDIX I

The non zero terms of the matrix $[K_{ij}]$ are given by the expression below and the parameters A, B, C, p and q are given in the table.

$$K_{ij} = A[B(1-\upsilon)M_p + C\upsilon M_q]\ 2G$$

i,j	A	B	C	p	q
1,1	-2	-1	1	3	1
1,4	24	-1	3	5	14
1,6	24	-1	1	6	4
1,15	24	0	1	-	4
2,2	8	-1	1	5	14
2,7	192	1	-3	7	8
2,9	576	1	-5	10	16
2,13	8	0	1	-	4
2,18	-576	0	1	-	8
2,20	-576	0	1	-	9
3,3	8	-1	1	6	4
3,8	192	1	-3	7	8
3,10	576	1	-1	11	9
3,12	8	0	1	-	4
3,17	-576	0	1	-	9
3,19	-576	0	1	-	8
4,4	72	1	-5	10	16
4,6	24	1	-3	7	8
4,15	-72	0	1	-	8
5,5	48	1	-3	7	8
5,14	-144	0	1	-	8
5,16	-144	0	1	-	9
6,4	24	1	-3	7	8
6,6	72	1	1	11	9
6,15	-72	0	1	-	9
7,7	576	-1	3	28	19
7,9	576	-1	5	27	18
7,18	1728	0	1	-	19
7,20	2880	0	1	-	20
8,8	576	-1	5	27	18
8,10	576	-1	3	28	19
8,17	1728	0	1	-	19
8,19	2880	0	1	-	18
9,7	192	-1	5	27	18
9,9	960	-1	7	21	29
9,18	960	0	1	-	18
9,20	576	0	1	-	19
10,8	192	-1	3	28	19
10,10	960	-1	1	22	20
10,17	960	0	1	-	20
10,19	576	0	1	-	19

i,j	A	B	C	p	q
11,5	24	0	1	-	4
11,11	2	1	-1	3	2
11,14	24	-1	1	5	4
11,16	24	-1	1	6	4
12,3	8	0	1	-	4
12,8	-576	0	1	-	8
12,10	-576	0	1	-	9
12,12	8	-1	1	5	4
12,17	192	1	-3	7	9
12,19	576	1	-1	10	8
13,2	8	0	1	-	4
13,7	-576	0	1	-	9
13,9	-576	0	1	-	8
13,13	8	-1	1	6	15
13,18	192	1	-3	7	9
13,20	576	1	-5	11	17
14,5	-72	0	1	-	8
14,14	72	1	-1	10	8
14,16	24	1	-3	7	9
15,4	-144	0	1	-	8
15,6	-144	0	1	-	9
15,15	48	1	-3	7	9
16,5	-72	0	1	-	9
16,14	24	1	-3	7	9
16,16	72	-1	5	11	17
17,8	1728	0	1	-	19
17,10	2880	0	1	-	20
17,17	576	-1	5	28	20
17,19	576	1	3	27	19
18,7	1728	0	1	-	19
18,9	2880	0	1	-	18
18,18	576	-1	3	27	19
18,20	576	-1	5	28	20
19,8	960	0	1	-	18
19,10	576	0	1	-	19
19,17	192	-1	3	27	19
19,19	960	-1	1	21	18
20,7	960	0	1	-	20
20,9	576	0	1	-	19
20,18	192	-1	5	28	20
20,20	960	-1	7	22	25

APPENDIX I
(continued)

$$M_p = \alpha_p \left[\beta_p E(k) + \gamma_p K(k)\right]$$

p	α_p	β_p	γ_p
1.	$2/a^3k^2$	-1	$+1$
2.	$2/ab^2k^2$	$+1$	$-k'^2$
3.	$2/a^3k'^2$	-1	0
4.	$2/a^3b^2k^4$	$1+k'^2$	$-2k'^2$
5.	$2/a^5k^2k'^2$	$1-2k^2$	$-k'^2$
6.	$2/a^5k^2k'^4$	$-1-k^2$	k'^2
7.	$2/a^7k^4k'^4$	$-2(k'^2+k^4)$	$k'^2(2-k^2)$
8.	$2/3a^5b^2k^6$	$3+5k'^2+2k^2k'^2$	$-k'^2(8+k^2)$
9.	$2/3a^3b^4k^6$	$3k^2k'^2+10k^2-8$	$8k'^2-9k^2k'^2$
10.	$2/3a^7k^4k'^2$	$2+3k^2-8k^4$	$-2(2k^2+1)k'^2$
11.	$2/3a^7k^4k'^4$	$3k^2+(2-10k^2)/k'^2$	$2(3k^2-1$
12.	$2/3a^7k^2k'^4$	$8k^2k'^2+5k^2-3$	$(3k'^2-k^2)k'^2$
13.	$2/3a^7k^2k'^6$	$2k^2k'^2+5k^2+3$	$-(k^2+3)k'^2$
14.	$2/3a^5k^4$	$-2(1+k^2)$	$2+k^2$
15.	$2/3ab^4k^4$	$2(2k^2-1)$	$k'^2(2-3k^2)$
16.	$2/15a^7k^6$	$-(8k^4+7k^2+8)$	$4k^4+3k^2+8$
17.	$2/15ab^6k^6$	$23k^4-23k^2+8$	$-k'^2(15k^4-19k^2+8)$
18.	$2/15a^7b^2k^8$	$15+33k'^2+17k^2k'^2+8k^4k'^2$	$-4k'^2(k^4+2k^2+12)$
19.	$2/3a^5b^4k^8$	$18k^2-16+8k^2k'^2-2k^2k'^4$	$k'^2(16-17k^2+k^2k'^2)$
20.	$2/15a^3b^6k^8$	$73k^4-113k^2+48-15k^2k'^4$	$-k'^2(60k^4-104k^2+48)$
21.	$2/15a^9k^6k'^2$	$8+9k^2+16k^4-48k^6$	$-k'^2(24k^4+13k^2+8)$
22.	$2/15a^9k^8k'^8$	$40k^2k'^2-48k^2+88k^4k'^2-15k^4k'^4$	$k'^2(16k^4-45k^4k'^2+8k^2)$
23.	$2/3a^9k^6k'^6$	$2k^2k'^4+4k^2k'^2-24k^2-16+16/k'^2$	$11k^2k'^2-8k^2-k^2k'^4$

APPENDIX I
(continued)

p	α_p	β_p	γ_p
24.	$2/3a^9k^4k'^4$	$16k^4k'^2+8k^4-4k^2-2$	$k'^2(2+5k^2-8k^4)$
25.	$2/105ab^8k^8$	$8(2k^2-1)(6-11k^2k'^2)$	$k'^2(105k^4k'^2+88k^4-160k^2+48)$
26.	$2/3a^9k^4k'^6$	$8-2k'^2-3k^2k'^2-8k^2k'^4$	$2k'^2(2k^2k'^2-k'^2-2)$
27.	$2/3a^9k^6k'^4$	$8k^4k'^2+3k^2k'^2-2k^2-8$	$k'^2(4k^2k'^2+5k'^2+3)$
28.	$2/3a^9k^6k'^4$	$6k^4-3k^2+16-8/k'^2$	$3k^2k'^2+12k^2-8$
29.	$2/105a^9k^8$	$8(1+k^2)(-6k^4+k^2-6)$	$24k^6+17k^4+16k^2+48$

APPENDIX II

The following are the expressions for K_2 and K_3 corresponding to each term in the stress function series.

a_{00} and b_{00}

$$K_2 = \frac{8G\pi^{\frac{1}{2}}}{(ab)^{3/2}\,\phi^{\frac{1}{4}}}\,(a_{00}\,b\cos\phi + b_{00}\,a\sin\phi)$$

$$K_3 = \frac{8G\pi^{\frac{1}{2}}}{(ab)^{3/2}\,\phi^{\frac{1}{4}}}\,(1-\nu)\,(b_{00}\,b\cos\phi - a_{00}\,a\sin\phi)$$

a_{10} and b_{10}

$$K_2 = \frac{-32G\pi^{\frac{1}{2}}}{(ab)^{3/2}\,\phi^{\frac{1}{4}}}\,(a_{10}\,\frac{b}{a}\cos^2\phi + b_{10}\sin\phi\cos\phi)$$

$$K_3 = \frac{32G\pi^{\frac{1}{2}}}{(ab)^{3/2}\,\phi^{\frac{1}{4}}}\,(1-\nu)\,(a_{10}\sin\phi\cos\phi - b_{10}\,\frac{b}{a}\cos^2\phi)$$

a_{01} and b_{01}

$$K_2 = \frac{-32G\pi^{\frac{1}{2}}}{(ab)^{3/2}\,\phi^{\frac{1}{4}}}\,(a_{01}\sin\phi\cos\phi + b_{01}\,\frac{a}{b}\sin^2\phi)$$

$$K_3 = \frac{32G\pi^{\frac{1}{2}}}{(ab)^{3/2}\,\phi^{\frac{1}{4}}}\,(1-\nu)\,(a_{01}\,\frac{a}{b}\sin^2\phi - b_{01}\sin\phi\cos\phi)$$

a_{11} and b_{11}

$$K_2 = \frac{192G\pi^{\frac{1}{2}}}{(ab)^{3/2}\,\phi^{\frac{1}{4}}}\,(\frac{a_{11}}{a}\sin\phi\cos^2\phi + \frac{b_{11}}{b}\sin^2\phi\cos\phi)$$

$$K_3 = \frac{192G\pi^{\frac{1}{2}}}{(ab)^{3/2}\,\phi^{\frac{1}{4}}}\,(1-\nu)\,(\frac{b_{11}}{a}\sin\phi\cos^2\phi - \frac{a_{11}}{b}\sin^2\phi\cos\phi)$$

a_{20} and b_{20}

$$K_2 = \frac{192G\pi^{\frac{1}{2}}}{(ab)^{3/2}\,\phi^{\frac{1}{4}}}\left(a_{20}\frac{b}{a^2}\cos^3\phi + b_{20}\frac{1}{a}\sin\phi\cos^2\phi\right)$$

$$K_3 = \frac{192G\pi^{\frac{1}{2}}}{(ab)^{3/2}\,\phi^{\frac{1}{4}}}(1-\nu)\left(b_{20}\frac{b}{a^2}\cos^3\phi - a_{20}\frac{1}{a}\sin\phi\cos^2\phi\right)$$

a_{02} and b_{02}

$$K_2 = \frac{192G\pi^{\frac{1}{2}}}{(ab)^{3/2}\,\phi^{\frac{1}{4}}}\left(a_{02}\frac{1}{b}\sin^2\phi\cos\phi + b_{02}\frac{a}{b^2}\sin^3\phi\right)$$

$$K_3 = \frac{192G\pi^{\frac{1}{2}}}{(ab)^{3/2}\,\phi^{\frac{1}{4}}}(1-\nu)\left(b_{02}\frac{1}{b}\sin^2\phi\cos\phi - a_{02}\frac{a}{b^2}\sin^3\phi\right)$$

a_{21} and b_{21}

$$K_2 = \frac{-1536G\pi^{\frac{1}{2}}}{(ab)^{3/2}\,\phi^{\frac{1}{4}}}\left(a_{21}\frac{1}{a^2}\sin\phi\cos^3\phi + b_{21}\frac{1}{ab}\sin^2\phi\cos^2\phi\right)$$

$$K_3 = \frac{1536G\pi^{\frac{1}{2}}}{(ab)^{3/2}\,\phi^{\frac{1}{4}}}(1-\nu)\left(a_{21}\frac{1}{ab}\sin^2\phi\cos^2\phi - b_{21}\frac{1}{a^2}\sin\phi\cos^3\phi\right)$$

a_{12} and b_{12}

$$K_2 = \frac{-1536G\pi^{\frac{1}{2}}}{(ab)^{3/2}\,\phi^{\frac{1}{4}}}\left(a_{12}\frac{1}{ab}\sin^2\phi\cos^2\phi + b_{12}\frac{1}{b^2}\sin^3\phi\cos\phi\right)$$

$$K_3 = \frac{1536G\pi^{\frac{1}{2}}}{(ab)^{3/2}\,\phi^{\frac{1}{4}}}(1-\nu)\left(a_{12}\frac{1}{b^2}\sin^3\phi\cos\phi - b_{12}\frac{1}{ab}\sin^2\phi\cos^2\phi\right)$$

a_{30} and b_{30}

$$K_2 = \frac{-1536G\pi^{\frac{1}{2}}}{(ab)^{3/2}\,\phi^{\frac{1}{4}}}\left(a_{30}\frac{b}{a^3}\cos^4\phi + b_{30}\frac{1}{a^2}\sin\phi\cos^3\phi\right)$$

$$K_3 = \frac{1536G\pi^{\frac{1}{2}}}{(ab)^{3/2}\,\phi^{\frac{1}{4}}}(1-\nu)\left(a_{30}\frac{1}{a^2}\sin\phi\cos^3\phi - b_{30}\frac{b}{a^3}\cos^4\phi\right)$$

a_{03} and b_{03}

$$K_2 = \frac{-1536G\pi^{\frac{1}{2}}}{(ab)^{3/2}\,\phi^{\frac{1}{4}}}\left(a_{03}\,\frac{1}{b^2}\,\sin^3\phi\,\cos\phi + b_{03}\,\frac{a}{b^3}\,\sin^4\phi\right)$$

$$K_3 = \frac{1536G\pi^{\frac{1}{2}}}{(ab)^{3/2}\,\phi^{\frac{1}{4}}}\,(1-\nu)\,\left(a_{03}\,\frac{a}{b^3}\,\sin^4\phi - b_{03}\,\frac{1}{b^2}\,\sin^3\phi\,\cos\phi\right)$$

$$\phi = a^2\,\sin^2\phi + b^2\,\cos^2\phi$$